The Astrophysical Journal, 597:494–512, 2003 November 1

CHANDRA/VERY LARGE ARRAY FOLLOW-UP OF TeV J2032+4131, THE ONLY UNIDENTIFIED TeV GAMMA-RAY SOURCE

Yousaf M. Butt,[1] Paula Benaglia,[2] Jorge A. Combi,[2] Michael Corcoran,[3] Thomas M. Dame,[1] Jeremy Drake,[1] Marina Kaufman Bernadó,[2] Peter Milne,[4] Francesco Miniati,[5] Martin Pohl,[6] Olaf Reimer,[6] Gustavo E. Romero,[2] and Michael Rupen[7]

Received 2003 February 18; accepted 2003 June 19

ABSTRACT

The High Energy Gamma Ray Astronomy (HEGRA) Cerenkov telescope array group recently reported a steady and extended unidentified TeV gamma-ray source lying at the outskirts of Cygnus OB2. This is the most massive stellar association known in the Galaxy, estimated to contain ~2600 OB-type members alone. It has been previously argued that the large-scale shocks and turbulence induced by the multiple interacting supersonic winds from the many young stars in such associations may play a role in accelerating Galactic cosmic rays. Indeed, Cyg OB2 also coincides with the nonvariable MeV–GeV range unidentified EGRET source, 3EG 2033+4118. We report on the near-simultaneous follow-up observations of the extended TeV source region with the *Chandra X-Ray Observatory* and the Very Large Array radio telescope, obtained in order to explore this possibility. Analysis of the CO, H I, and *IRAS* 100 μm emissions shows that the TeV source region coincides with an outlying subgroup of powerful OB stars that have evacuated or destroyed much of the ambient atomic, molecular, and dust material and that may be related to the very high energy emissions. An interesting supernova-remnant–like structure is also revealed near the TeV source region in the CO, H I, and radio emission maps. Applying a numerical simulation that accurately tracks the radio to gamma-ray emission from primary hadrons as well as primary and secondary $e^{\pm}$, we find that the broadband spectrum of the TeV source region favors a predominantly nucleonic—rather than electronic—origin for the high-energy flux, although deeper X-ray and radio observations will help confirm this. A very reasonable, ~0.1%, conversion efficiency of Cyg OB2's extreme stellar wind mechanical luminosity to nucleonic acceleration to ~PeV (10^{15} eV) energies is sufficient to explain the multifrequency emissions.

Subject heading: gamma rays: observations

1. INTRODUCTION

The astrophysical sites where Galactic cosmic-ray (GCR) nuclei gain their extreme energies (up to $\sim 10^{15}$ eV nucleon^{-1}) continue to defy identification. The expanding shock waves of supernova remnants (SNRs) have long been conjectured to be the accelerators of GCRs based mostly on energetic and spectral consistency arguments (e.g., Ginzburg & Syrovatskii 1969; Drury et al. 2001). Recent observations from ground-based Cerenkov gamma-ray telescopes have provided direct evidence of TeV range *electrons* in individual SNRs (e.g., Muraishi et al. 2000), although the situation for nuclei remains more confused (e.g., Reimer & Pohl 2002; Butt et al. 2002; Torres et al. 2003; Erlykin & Wolfendale 2003). Using certain theoretical models, it has been possible to interpret the multifrequency emissions from some young SNRs in terms of either nuclear or electron sources, depending on the precise parameters adopted (e.g., Gaisser, Protheroe, & Stanev 1998; Ellison, Berezhko, & Baring 2000; Berezhko, Puehlhofer, & Völk 2003).

However, whether or not individual SNRs are sources of GCR nuclei, it is nonetheless important to explore the related (i.e., shock driven) acceleration processes thought to operate in conglomerates of SNRs and/or massive stars. Bruhweiler et al. (1980) and Kafatos, Bruhweiler, & Sofia (1981), among others (e.g., McCray & Kafatos 1987; Mac Low & McCray 1988), have pointed out that since most supernova (SN) explosions are core-collapse SNe of massive progenitors ($M \gtrsim 8\ M_{\odot}$), and since such progenitor stars are typically formed in associations, it is plausible that the resulting "superbubbles" (Heiles 1979), characterized by the collective shocks induced by close-by and time-correlated SN explosions, should be even more promising GCR source sites. For recent reviews, see, e.g., Bykov (2001) and Parizot (2003). From separate considerations of the spallogenic origin of the light elements LiBeB, Ramaty, Lingenfelter, & Kozlovsky (2001) and Alibés, Labay, & Canal (2002) also favor the superbubble hypothesis for the origin of GCRs. An important ingredient of such superbubble GCR acceleration models is the additional MHD turbulence induced by the multiple, interacting, supersonic winds blowing from the many young and massive stars present in such associations (e.g., Bykov & Fleishman 1992; Toptygin 1999; Bykov & Toptygin 2001).

More than 20 years ago, Cassé & Paul (1980) proposed that the shocked region at the boundary between even a single massive star's stellar wind and the interstellar medium (ISM) could accelerate nuclei to GCR energies without invoking SNR shocks at all. They pointed out that the

[1] Harvard-Smithsonian Center for Astrophysics, 60 Garden Street, Cambridge, MA 02138; corresponding author: ybutt@cfa.harvard.edu.
[2] Instituto Argentino de Radioastronomía, Casilla de Correo 5, Villa Elisa, 1894 Buenos Aires, Argentina.
[3] Universities Space Research Association, 7501 Forbes Boulevard, Suite 206, Seabrook, MD 20706; and Laboratory for High Energy Astrophysics, NASA Goddard Space Flight Center, Greenbelt, MD 20771.
[4] Los Alamos National Laboratory (T-6), MS B-277, Los Alamos, NM 87545.
[5] Max-Planck-Institut für Astrophysik, Karl-Schwarzschild-Strasse 1, D-85741 Garching, Germany.
[6] Institut für Theoretische Physik, Ruhr-Universität Bochum, D-44780 Bochum, Germany.
[7] National Radio Astronomy Observatory, Socorro, NM 87801.

integrated mechanical power of a massive star's wind over its lifetime is comparable to the energy liberated in the final SN explosion ($\sim 10^{51}$ ergs). Cesarsky & Montmerle (1983) went further by demonstrating how the turbulent interacting supersonic stellar winds of the many young OB stars in some associations could dominate the GCR acceleration process for the first 4–6 Myr, even before the first SNe begin to explode. In fact, they suggested that such "cumulative" OB association stellar winds may be even more efficient than individual SNRs in accelerating GCRs for two reasons: the stellar wind shocks will be turbulent on both sides of the shock interface (thus speeding up the acceleration process), and, since there is continuous energy input, the shock velocity can remain higher for longer than in the impulsively powered SNR shocks.

Of course, it is possible that all three shock acceleration processes, among other unrelated mechanisms (e.g., Dar & Plaga 1999), are responsible for GCR acceleration in varying degrees: individual SNRs (e.g., Torres et al. 2003; Erlykin & Wolfendale 2003), correlated SNRs and young stars in superbubbles (e.g., Montmerle 1979; Kafatos et al. 1981; Bykov 2001), and multiple, interacting, stellar winds in massive OB associations (e.g., Cesarsky & Montmerle 1983).

Unfortunately, the direct and firm identification of even a *single* nucleonic GCR acceleration site has continued to elude observers to date. In this context, the recent report by the High Energy Gamma Ray Astronomy (HEGRA) collaboration of an extended and steady TeV source within the boundary of the Cyg OB2 stellar association (Rowell et al. 2002; Aharonian et al. 2002; Horns & Rowell 2003) provides an ideal opportunity to test the stellar association hypothesis of GCR origin. The low latitude of the source, its $\sim 11'$ (Gaussian best fit) extension, and its lack of variability all point to a Galactic origin.[8]

At $(4\text{–}10) \times 10^4\ M_\odot$, Cyg OB2 is the most massive OB association known in the Galaxy; the reader is referred to, e.g., Reddish, Lawrence, & Pratt (1966), Knödlseder (2000, 2003), Comerón et al. (2002), and Uyaniker et al. (2001) for useful overviews. Although it houses some of the most massive and luminous stars in the Galaxy, including the only two extreme O3 If* type stars known in the northern hemisphere (stars 7 and 22-A; Knödlseder 2003), Cyg OB2 is also a rather compact association: at 1.7 kpc it has a diameter of ~ 60 pc or $\sim 2^\circ$. This implies a tremendous mechanical power density from the cumulative stellar winds of its ~ 2600 OB star members: Lozinskaya, Pravdikova, & Finoguenov (2002) estimate that an average of a few $\times\ 10^{39}$ ergs s^{-1} must have been continuously released over the past ~ 2 Myr in this region.

Such extreme characteristics make Cyg OB2 a prime candidate for investigating the stellar association hypothesis of the acceleration of GCRs. Already in 1992, White & Chen (1992) predicted that Cyg OB2 ought to be marginally detectable in MeV–GeV gamma rays by the EGRET instrument based on a model considering the summed $\pi^0 \rightarrow \gamma\gamma$ emission from the interactions of energetic nuclei accelerated by just its four most luminous members. That the nonvariable gamma-ray source 3EG J2033+4118 (2EG J2033+4112/GRO J2032+40; Hartman et al. 1999) was found to be centered on Cyg OB2 argues strongly in favor of a physical association (White & Chen 1992; Chen, White, & Bertsch 1996), although the precise physics of the gamma-ray production may be subject to debate. For instance, it has been argued that the binary system Cyg OB2 No. 5 may also, by itself, be contributing significant gamma-ray flux through inverse Compton (IC) upscattering of ambient photons by the relativistic electrons known to exist in its colliding wind region (Benaglia et al. 2001; Contreras et al. 1997). More broadly speaking, several OB associations are found to be coincident with unidentified EGRET sources, although it is in general difficult to be confident that the associations themselves are the source of the high-energy emissions (Romero, Benaglia, & Torres 1999).

In Figure 1 we show the stellar density plots of all *cataloged* OB member stars together with overlays indicating the positions of 3EG J2033+4118 and TeV J2032+4131; interestingly, the TeV source coincides with a distinct subgroup of outlying OB stars. Note that many stars in Cyg OB2 remain undetected and uncataloged because of high visual extinction in this direction (e.g., Comerón et al. 2002). Six cataloged O and eight cataloged B stars lie within the reported extent of the TeV source, but again these numbers should be considered strict lower limits. Their parameters and locations are detailed in Table 1.

2. OBSERVATIONS

The intentions of our follow-up X-ray and radio observations were twofold: first, to attempt to identify any likely counterparts of the TeV emission (since, e.g., an SNR expanding within a hot, low-density medium such as an OB association leaves little or no radio/optical signatures [Chu 1997], X-ray observations can be very enlightening); and second, to measure, or place stringent limits on, the diffuse X-ray and radio emission and thus attempt to constrain whether nuclei or electrons dominate the TeV gamma-ray production.

2.1. *Chandra*

We obtained a 5 ks Director's Discretionary Time (DDT) *Chandra* observation of TeV J2032+4131

$$\alpha_{\mathrm{J2000.0}} = 20^{\mathrm{h}}32^{\mathrm{m}}07^{\mathrm{s}} \pm 9\overset{\mathrm{s}}{.}2 \pm 2\overset{\mathrm{s}}{.}2\ ,$$
$$\delta_{\mathrm{J2000.0}} = +41^\circ 30' 30'' \pm 102'' \pm 24''\ ,$$

radius $\sim 5\overset{'}{.}6$; Aharonian et al. 2002) starting on 2002 August 11 19:51 GMT (observation ID 4358). The data were obtained with the ACIS instrument in very faint mode with chips I0, I1, I2, I3, S2, and S5. The $\sim 11'$ TeV source region was centered on the $\sim 16\overset{'}{.}9 \times 16\overset{'}{.}9$ active region of the 4 ACIS-I chips. This field of view comfortably accommodated the $\sim \pm 2'$ positional error quoted by HEGRA. The data were processed with ASCDS, version 6.8.0, of the *Chandra* telemetry processing pipelines and were analyzed with CIAO, version 2.0. A raw (binned by 8 pixels) image of the ACIS-I chips showing the HEGRA source region is illustrated in Figure 2.

A search for point sources using the *wavdetect* tool resulted in 19 sources above 2.5 σ (15 above 3 σ; Table 2), some associated with already cataloged stars in the region

[8] However, the extragalactic alternative cannot be altogether eliminated: an extended extragalactic TeV source, the starburst galaxy NGC 253, has been recently reported by the CANGAROO collaboration (Itoh et al. 2002, 2003), and a possible explanation in terms of cosmic rays illuminating the core regions of massive stars there has been put forth by Romero & Torres (2003; see also Anchordoqui, Romero, & Combi 1999).

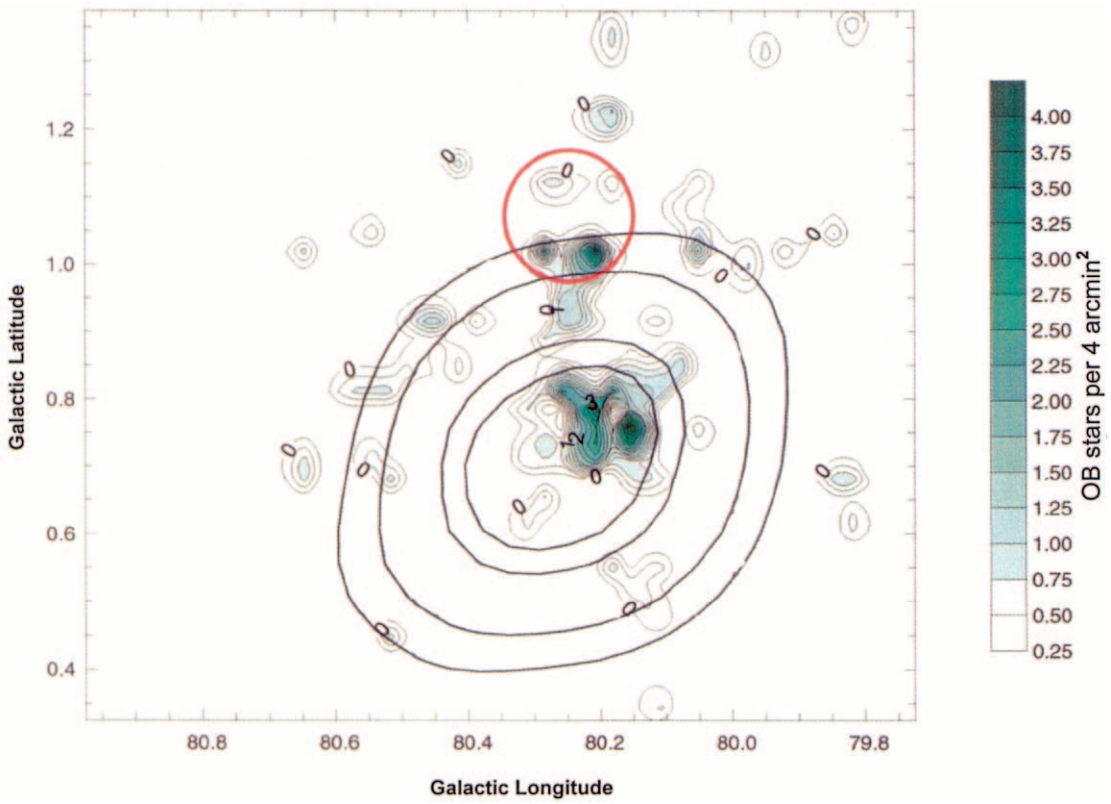

FIG. 1.—Distribution of all 110 *cataloged* OB stars in Cyg OB2 shown as a surface density plot (stars per 4 arcmin^2). Note that many stars in Cyg OB2 remain uncataloged; the total number of OB stars alone is expected to be ~2600 (Knödlseder 2003). Although the extinction pattern toward Cyg OB2 may control the observed surface density of OB stars, our analysis assumes that the observed distribution of OB stars tracks the actual distribution. The thick contours show the location probability contours (successively, 50%, 68%, 95%, and 99%) of the nonvariable MeV–GeV range EGRET gamma-ray source 3EG 2033+4118 (Hartman et al. 1999). The red circle outlines the 5′.6 radius extent of the diffuse and steady TeV source, TeV J2032+4131, reported by HEGRA (Rowell et al. 2002; Aharonian et al. 2002).

(Table 3). The source positions have also been overlaid on the ACIS detector image in Figure 3. None of the point sources detected are particularly prominent in X-rays, and none present sufficient counts to enable detailed spectral analysis. However, since the TeV source is known to be extended (with ~3 σ confidence), we were particularly interested in investigating the diffuse X-ray emission.[9] We first looked for diffuse structure by adaptively smoothing, using the tool *csmooth*,[10] an image from which the events associated with the detected point sources had been removed. The result of this smoothing is illustrated in Figure 3, in which the detected point sources have been overlaid in green. The diffuse X-ray emission within the region of the TeV source is very weak and shows no significant enhancement over neighboring regions. The smoothed image is brightest toward the southeast of the 5′.6 radius HEGRA TeV source region, in the direction of the core of Cyg OB2. We note that the area just northwest of the brightest diffuse region in the southeast corner also tends to harbor most of the detected point sources. A total of 3837 counts (0.3–10 keV in grades 0, 2, 3, 4, and 6) were detected in the TeV source region, of which 265 can be attributed to pointlike sources.

Pulse-height spectra were extracted and telescope response functions calculated for the TeV source region (with point sources removed) using the *acisspec* script. Resulting spectra were analyzed using the SHERPA fitting engine. In order to properly analyze faint spectra of diffuse emitting regions, it is first necessary to account for the particle background that can give rise to significant events in the ACIS detector. A detailed study of the ACIS background has found that, outside of background flare events, both dark-Moon observations (from which cosmic X-rays are occulted) and observations made with ACIS in the stowed position—out of the focal plane—are characterized by a spectrum of cosmic-ray–induced events that appears stable over long periods and that only exhibits relatively small secular changes in overall intensity due to modulation by global solar activity levels (Markevitch et al. 2003). We adopted the methods developed by Markevitch and coworkers to estimate the background based on high

[9] Mukerjee et al. (2003) have recently presented a study of this source under the assumption that the TeV emission is not extended. However, a recent analysis of new HEGRA data from 2002 has confirmed the extended nature of TeV J2032+4131 at the >5 σ level (Horns & Rowell 2003). It remains possible, however, that several distinct pointlike TeV sources could be masquerading as a single extended source, given the HEGRA point-spread function. Mukerjee and collaborators have also asserted that the possibly associated source 3EG J2033+4118 is variable under the convention of McLaughlin et al. (1996), whereas this source is known to be nonvariable under all accepted variability schemes, including that of McLaughlin and collaborators (Tompkins 1999; Torres et al. 2001; M. McLaughlin 2003, private communication; $V = 0.4$). There is no indication of source variability beyond the inherent systematics in the method and data itself: it is more than 3 σ from the average active galactic nucelus variability.

[10] See http://cxc.harvard.edu/ciao/ahelp/csmooth.html.

TABLE 1
OB STARS SURROUNDING THE TeV SOURCE FOR $d \leq 9'$

Name	R.A. (J2000.0)	Decl. (J2000.0)	Spectral Class[a]	r (pc)	$\log(\dot{M}_{\rm exp})$[b]
Cyg OB2 560	20 31 49.74	41 28 26.9	O9.5 V	2.0	−6.564
VI Cyg 4	20 32 13.82	41 27 12.0	O7 III((f))	1.7	−5.567
Cyg OB2 14	20 32 16.5	41 25 36	O...	2.4	−6.367
Cyg OB2 31	20 32 16.62	41 25 36.4	O9 V	2.4	−6.367
Cyg OB2 516	20 32 25.59	41 24 51.9	O5.5 V	3.2	−5.432
Cyg OB2 15	20 32 27.5	41 26 15	O8 V	2.7	−6.099
Cyg OB2 30	20 32 27.66	41 26 22.11	O8 V	2.7	−6.099
A43[c]	20 32 38.5	41 25 13.0	O...	3.9	−6.367
[MT91] 299[d]	20 32 38.66	41 25 13.7	O7.5 V	3.9	−6.003
VI Cyg 6	20 32 45.44	41 25 37.51	O8 V:	4.2	−6.099
NSV 13126	20 31 22.02	41 31 28.4	B1 Ib:	4.4	−5.9
Cyg OB2 205	20 31 55.9	41 33 04	B1.5 V	1.9	−6.7
Cyg OB2 210	20 31 56.4	41 31 48	B1.5 V	1.2	−6.7
Cyg OB2 545	20 32 03.3	41 25 12	B0.5 :V	2.4	−6.4
[MT91] 213[d]	20 32 12.8	41 22 26	B0 Vp	1.5	−6.2
[MT91] 215[d]	20 32 13.2	41 27 32	B1 V	1.3	−6.6
Cyg OB2 500	20 32 25.8	41 29 39	B1 V	1.7	−6.6
Cyg OB2 21	20 32 27.4	41 28 52	B1 III	1.9	−6.0
Cyg OB2 502	20 32 27.85	41 28 52	B0.5 V	1.9	−6.4
Cyg OB2 492	20 32 36.8	41 23 26	B1 V	4.3	−6.6

NOTES.—Units of right ascension are hours, minutes, and seconds, and units of declination are degrees, arcminutes, and arcseconds. Stars are selected from the SIMBAD database, Chen et al. 1996, Comerón et al. 2002, and Massey & Thompson 1991.

[a] From SIMBAD.

[b] Computed from Vink, de Koter, & Lamers 2001, if stellar luminosities, masses, and effective temperatures are from Vacca, Garmany, & Schull 1996 and terminal velocities are from Prinja, Barlow, & Howarth 1990.

[c] Comerón et al. 2002.

[d] Massey & Thompson 1991.

signal-to-noise ratio background observations obtained with ACIS in the stowed position.[11] A background spectrum was obtained for the 5′.6 radius HEGRA TeV source region, and this was subtracted from the observed spectrum prior to spectral analysis. In addition to this background correction, we also included the effects of the decrease in the quantum efficiency of the ACIS detector as a result of possible filter contamination buildup using the ACISABS model.[12]

Unfortunately, we found that because of the low statistics obtained, the residual TeV source region X-ray spectrum could be equally well represented by optically thin plasma models (the Mewe-Kaastra-Liedahl (MEKAL) model) or nonthermal power laws. In the case of the former, no constraints were able to be placed on the metallicity parameter: models with metallicity in the range 0–1.2 times the solar photospheric abundances of Anders & Grevesse (1989) were statistically acceptable, yielding reduced χ^2 values of about 0.9. Similar reduced χ^2 values were obtained for power-law models. The results of the parameter estimation process for these models are listed in Table 4. The spectrum and model fit for the optically thin plasma case are illustrated in Figure 4.

Based on the best-fit spectral models, we obtain a diffuse flux within the source region of 1.3×10^{-12} ergs cm^{-2} s^{-1} for the 0.5–2.5 keV bandpass and 3.6×10^{-12} ergs cm^{-2} s^{-1} for the 2.5–10 keV bandpass. These values are not sensitive to the type of model adopted; power-law and optically thin plasma best-fit models give the same result to within ∼5% within the allowed 1 σ parameter ranges for the different models. *Unfortunately, because both power-law and thermal-plasma models are equally acceptable, the flux values extracted above can only be taken as upper limits to the nonthermal component alone*. Consequently, in our quantitative modeling (§ 4) of the multiwavelength emissions, we have taken the measured (instrumental background-subtracted) X-ray flux as an upper limit to the X-ray emission associated with the TeV source. A deeper, ∼50 ks observation would yield sufficient counts to permit a reliable decomposition of the X-ray emission into thermal and power-law components.

Spectra were also extracted for different regions surrounding the TeV source region, including the brighter region to the southeast. The TeV source region showed no significant excess hardness compared to these other regions, and spectra were qualitatively very similar.

2.2. *Very Large Array B Configuration*

On the following day, 2002 August 12, we obtained an 8 minute 4.86 GHz Very Large Array (VLA)[13] exposure in the B configuration, sampling a 10′.24 × 10′.24 region centered at the TeV source (the half-power sensitivity region of the antenna has about a 9′ diameter in this configuration). In the B configuration, the VLA array is sensitive only to

[11] See http://asc.harvard.edu/ciao/threads/acisbackground.

[12] See http://asc.harvard.edu/ciao/threads/apply_acisabs.

[13] The VLA is operated by the National Radio Astronomy Observatory (NRAO), which is a facility of the National Science Foundation (NSF), operated under cooperative agreement by Associated Universities, Inc.

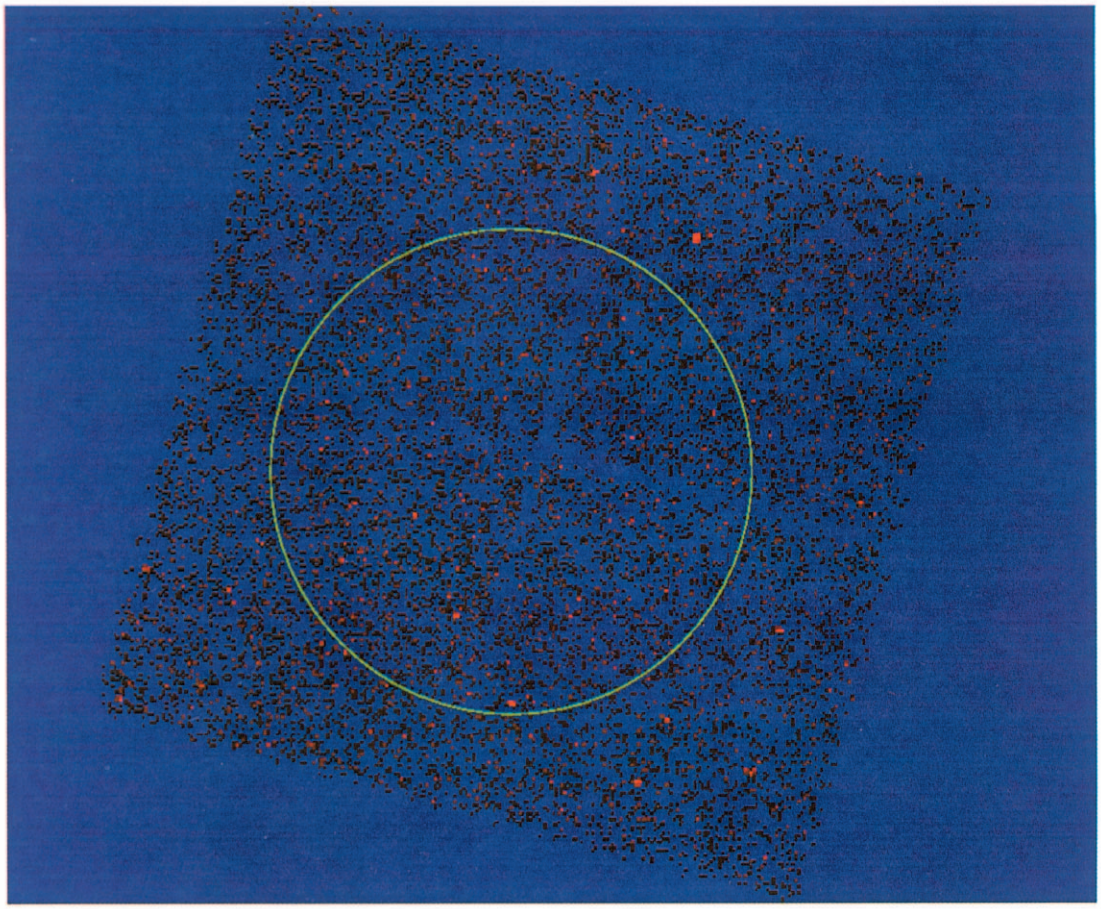

FIG. 2.—Raw 5 ks *Chandra* image of the 4 I-array chips (binned by 8 pixels). The green circle shows the 5′.6 radius extent of the diffuse TeV source, TeV J2032+4131, reported by HEGRA (Aharonian et al. 2002). The aim point is at the center of the circle, $\alpha(\mathrm{J2000.0}) = 20^{\mathrm{h}}32^{\mathrm{m}}07^{\mathrm{s}}$, $\delta(\mathrm{J2000.0}) = +41^{\circ}30'30''$. North is up, and east is to the left.

pointlike radio sources. We achieved an rms noise of 96 μJy beam^{-1} for a beam size (point-spread function) of $1''.50 \times 1''.42$ (FWHM), oriented 28° east of north. We detected no pointlike sources to the limiting flux in the region of interest sampled by the primary beam.

2.3. *VLA D Configuration*

Since the VLA B configuration data we obtained are not sensitive to any possible diffuse radio emission present in the TeV source region, we reanalyzed archival D configuration data at 1.489 GHz taken in 1984, from which we obtained an upper limit to diffuse emission of less than 200 mJy in the region of the TeV source (Fig. 5). Our analysis (§ 4) assumes no time variability of the source since 1984, consistent with the multiyear steadiness reported by HEGRA.

2.4. *ROSAT Position Sensitive Proportional Counter*

We reanalyzed 19.5 ks *ROSAT* Position Sensitive Proportional Counter (PSPC) data from 1993 April/May (sequence 900314; Waldron et al. 1998). We extracted a source spectrum from a ~12′ diameter circle centered on $\alpha_{\mathrm{J2000.0}} = 20^{\mathrm{h}}32^{\mathrm{m}}07^{\mathrm{s}}$, $\delta_{\mathrm{J2000.0}} = +41^{\circ}30'30''$, excluding obvious discrete sources. Unfortunately, the PSPC inner support ring runs through this region, which influences the results of our spectral fit. We used a nearby 12′ circular region to estimate the background. The net (background-subtracted) rate within the TeV source region was 0.107 ± 0.007 PSPC counts s^{-1}. An absorbed power-law fit yields an acceptable fit with a reduced χ^2 value of 0.72 for 17 degrees of freedom, with a photon index of 0.26, a normalization of 5×10^{-4}, $N(\mathrm{H}) = 0$, and a flux (0.2–2.4 keV) of 2×10^{-12} ergs cm^{-2} s^{-1}. A single-temperature absorbed thermal model did not yield an acceptable fit (reduced χ^2 of 2.49 for 17 degrees of freedom). We were able to generate an acceptable fit to the data using a two-component thermal model with two separate absorption components (reduced $\chi^2 = 0.79$ for 14 degrees of freedom). As in the *Chandra* analysis, a hardness image (0.5–2.0 keV) also did not reveal any significant excess hardness in the region of the TeV source. Since our analysis could not resolve the nonthermal versus thermal nature of the spectrum, the flux of 2×10^{-12} ergs cm^{-2} s^{-1} can be considered an upper limit to the nonthermal emission in the 0.2–2.4 keV band, in good agreement with the *Chandra* results.

2.5. *EGRET*

The more than 100 MeV source, 3EG J2033+4118, whose 95% and 99% confidence location contours overlap the extended TeV source region (Fig. 1), is a ~12 σ detection centered at $l = 80.^{\circ}27$, $b = +0.^{\circ}73$, with a radial positional

TABLE 2

POINTLIKE X-RAY SOURCES DETECTED IN THE TeV SOURCE REGION

Source ID	x	y	Error x	Error y	R.A. (J2000.0)	Decl. (J2000.0)	S/N	netB	Error netB
XS 04358B0_004	5055.43	4009.50	0.85	0.87	20 31 23.55	41 29 48.7	3.2	19	6
XS 04358B2_007	4825.85	3648.26	0.92	0.59	20 31 33.63	41 26 51.2	3.2	17	5
XS 04358B2_009	4743.82	3250.92	1.41	1.17	20 31 37.24	41 23 35.7	3.2	19	6
XS 04358B6_004	4732.06	2001.42	2.74	2.49	20 31 37.83	41 13 21.0	10.0	146	15
XS 04358B0_002	4592.83	4753.28	0.32	0.35	20 31 43.77	41 35 55.0	12.8	190	15
XS 04358B2_005	4422.18	3223.85	0.77	0.40	20 31 51.31	41 23 22.6	5.1	38	7
XS 04358B0_001	4408.75	4191.85	0.21	0.23	20 31 51.86	41 31 18.8	3.7	22	6
XS 04358B1_004	4304.17	4932.17	0.59	0.85	20 31 56.43	41 37 23.1	4.7	33	7
XS 04358B2_002	4067.34	3443.97	0.53	0.37	20 32 06.82	41 25 10.9	4.2	26	6
XS 04358B3_006	3907.58	3690.17	0.24	0.24	20 32 13.81	41 27 12.0	4.4	29	6
XS 04358B6_005	3884.06	1785.92	4.19	3.18	20 32 14.80	41 11 35.2	4.4	41	9
XS 04358B3_001	3792.98	3975.72	0.16	0.21	20 32 18.83	41 29 32.5	4.1	25	6
XS 04358B3_012	3592.20	3587.60	0.65	0.30	20 32 27.60	41 26 21.5	3.1	17	5
XS 04358B3_019	3184.15	3495.80	1.25	1.73	20 32 45.45	41 25 36.0	2.5	15	6
XS 04358B3_018	3031.55	3819.36	1.57	1.56	20 32 52.16	41 28 15.0	3.0	19	6
XS 04358B3_017	2956.44	3458.72	1.46	1.04	20 32 55.41	41 25 17.5	3.3	25	8
XS 04358B9_002	1648.67	2734.17	0.28	0.30	20 33 52.45	41 19 18.6	2.7	23	8
XS 04358B9_001	1643.83	2767.17	0.27	0.27	20 33 52.67	41 19 34.8	2.7	23	9
XS 04358B9_003	1630.75	2768.00	0.22	0.25	20 33 53.24	41 19 35.2	2.6	22	8

NOTES.—Units of right ascension are hours, minutes, and seconds, and units of declination are degrees, arcminutes, and arcseconds. The "S/N" column gives the signal-to-noise ratio of the detection. The "netB" column refers to the number of counts after background subtraction. The following column, "Error netB," gives the statistical error in this figure.

TABLE 3

CATALOGED STARS COINCIDENT WITH, OR NEARBY, THE POINTLIKE X-RAY SOURCES LISTED IN TABLE 4

Source ID	$r = 15''$	$r = 30''$	R.A. (J2000.0)	Decl. (J2000.0)	Object
XS 04358B0_004	...	...	...	...	...
XS 04358B2_007	...	...	...	...	...
XS 04358B2_009	[MT91] 115	[MT91] 115	20 31 37.38	41 23 35.5	*
	Assoc. Cyg OB2 581	Assoc. Cyg OB2 581	20 31 37.4	41 23 35	*
		Assoc. Cyg OB2 580	20 31 37.2	41 23 35	*
		[MT91] 114	20 31 37.20	41 23 55.4	*
XS 04358B6_004	NSV 13129	NSV 13129	20 31 37.50	41 13 21.2	*, O9:
	[TSA98] J203138.83+411324.74	[TSA98] J203138.83+411324.74	20 31 38.83	41 13 24.7	X
		1RXS J203140.1+411319	20 31 40.10	41 13 19.0	X
XS 04358B0_002	Assoc. Cyg OB2 195	Assoc. Cyg OB2 195	20 31 43.8	41 36 07	*
	[MT91] 136	[MT91] 136	20 31 43.72	41 36 07.6	*
XS 04358B0_005	Assoc. Cyg OB2 551	Assoc. Cyg OB2 551	20 31 51.4	41 23 23	*
	[MT91] 152	[MT91] 152	20 31 51.42	41 23 23.6	*
	2E 2031.1+4112	2E 2031.1+4112	20 31 50.9	41 23 19	X
XS 04358B0_001	[MT91] 150	[MT91] 150	20 31 50.91	41 31 17.5	*
	Assoc. Cyg OB2 208	Assoc. Cyg OB2 208	20 31 50.9	41 31 18	*
		[MT91] 162	20 31 54.48	41 31 13.5	*
XS 04358B1_004		Assoc. Cyg OB2 197	20 31 53.9	41 37 30	*
XS 04358B2_002		[MT91] 206	20 32 09.00	41 25 05.6	*
		Assoc. Cyg OB2 546	20 32 09.1	41 25 05	*
XS 04358B3_006	VI Cyg 4	VI Cyg 4	20 32 13.82	41 27 12.0	*, O7 III((f))
	[MT91] 213		20 32 12.8	41 27 26	*, B0 Vp
	[MT91] 215		20 32 13.2	41 27 32	*, B1 V
	[MT91] 221		20 32 14.3	41 27 41	*
XS 04358B6_005	...	...	...	...	...
XS 04358B3_001		Assoc. Cyg OB2 532	20 32 19.5	41 30 00	*
		[MT91] 233	20 32 19.35	41 30 01.0	*
XS 04358B3_012	Assoc. Cyg OB2 30	Assoc. Cyg OB2 30	20 32 27.66	41 26 22.1	*, O8 V
	Assoc. Cyg OB2 15	Assoc. Cyg OB2 15	20 32 27.5	41 26 15	*, O8 V
XS 04358B3_019	BD+40 4221	BD+40 4221	20 32 45.4	41 25 37	*
	VI Cyg 6	VI Cyg 6	20 32 45.44	41 25 37.5	*, O8 V:
		[MT91] 312	20 32 43.61	41 25 38.4	*
		Assoc. Cyg OB2 483	20 32 43.6	41 25 38	*
XS 04358B3_018	[MT91] 351	[MT91] 351	20 32 52.87	41 28 19.2	*
	Assoc. Cyg OB2 477	Assoc. Cyg OB2 477	20 32 52.9	41 28 19	*
XS 04358B3_017	[MT91] 360	[MT91] 360	20 32 54.88	41 25 15.6	*
XS 04358B9_002	...	...	...	...	...
XS 04358B9_001	...	...	...	...	...
XS 04358B9_003	...	...	...	...	...

NOTES.—Units of right ascension are hours, minutes, and seconds, and units of declination are degrees, arcminutes, and arcseconds. Objects marked with an asterisk signify cataloged stars. The spectral type is given when available. The two columns $r = 15''$ and $r = 30''$ give the search radius around each X-ray source. Some of the X-ray sources without counterparts may be young stars that have yet to be optically identified because of high extinction toward the Cyg direction. "X" stands for a previously detected X-ray source.

uncertainty $\theta_{95\%} = 0.^{\circ}28$ (Hartman et al. 1999). An elliptical fit by Mattox, Hartman, & Reimer (2001) yields the parameters $a = 18.'7$, $b = 15.'0$, $\phi = 67^{\circ}$, where a and b are the length of the semimajor and semiminor axes in arcminutes and ϕ is the position angle of the semimajor axis in degrees. 3EG J2033+4118 is classified as being a nonvariable source by Tompkins (1999), Torres et al. (2001), McLaughlin et al. (1996; $V = 0.61$ for 2EG J2033+4112), and M. McLaughlin (2003, private communication; $V = 0.4$ for 3EG J2033+4118).

At energies above 1 GeV, the narrower instrumental point-spread function of EGRET and the less dominant diffuse gamma-ray background usually enable better source locations for gamma-ray point sources. This is possible if the source spectrum falls less steeply than the spectrum of the diffuse gamma-ray emission above 1 GeV and if sufficient photons for an analysis are still available at the higher energies. Two compilations of gamma-ray sources at $E > 1$ GeV have been obtained that differ in subtle, but important, details: the GeV catalog of Lamb & Macomb (1997) and the *Compton Gamma Ray Observatory* (*CGRO*) catalog of Reimer, Dingus, & Nolan (1997). Only the sources GeV J2035+4214/GRO J2034+4203 from these two catalogs, respectively, could possibly be counterparts for the TeV source position, although it is highly unlikely based on the large positional offsets.

GeV J2035+4214 (Lamb & Macomb 1997).—This source at $l = 81.^{\circ}22$, $b = 1.^{\circ}02$ was detected with a significance of 6.6 σ and more than 1 GeV flux of $(8.1 \pm 1.5) \times 10^{-8}$ photons cm^{-2} s^{-1}, with position uncertainties for the elliptical fit at the 95% contour, $a = 25.'4$, $b = 17.'3$, and $\phi = 25^{\circ}$.

GRO J2034+4203 (Reimer et al. 1997).—This source at $l = 80.^{\circ}97$, $b = 1.^{\circ}04$ was detected with a significance of 5.8 σ and more than 1 GeV flux of $(5.7 \pm 1.3) \times 10^{-8}$ photons cm^{-2} s^{-1}, with 95% and 68% errors of $21'$ and $14'$, respectively.

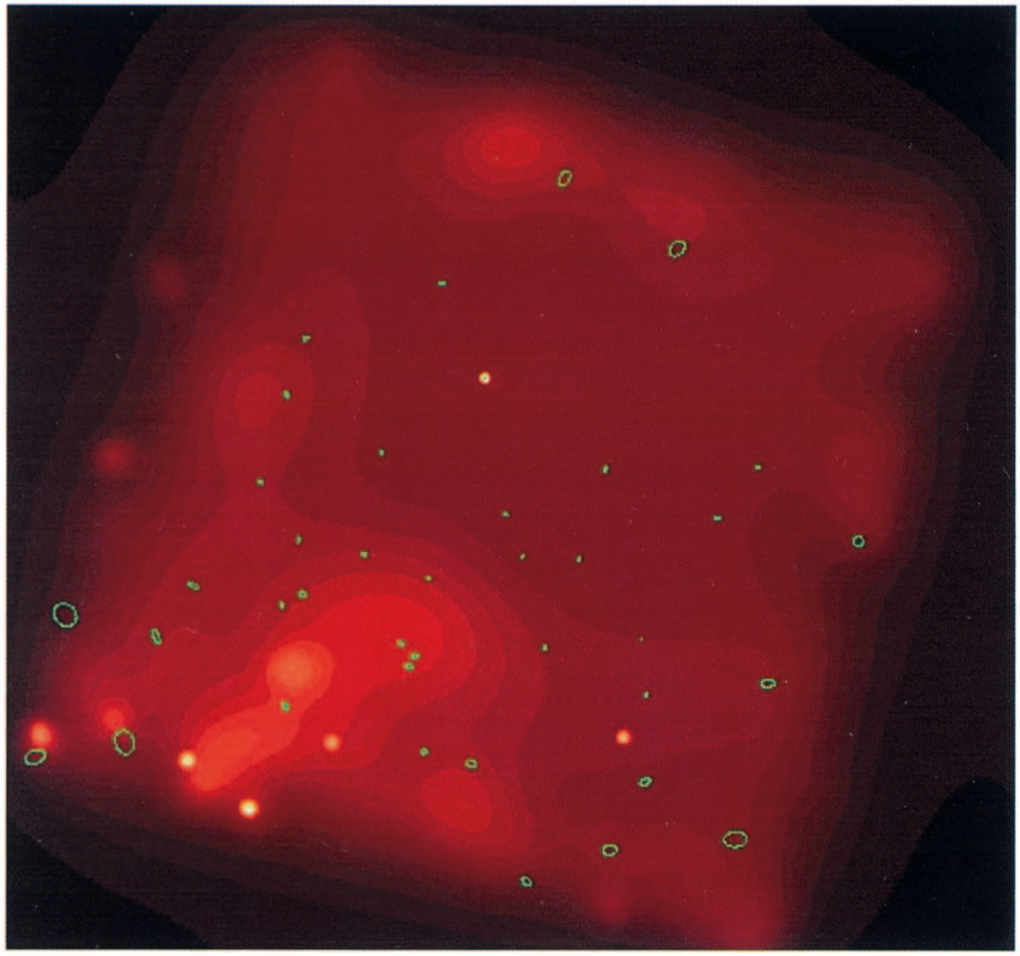

FIG. 3.—Adaptively smoothed X-ray image of the TeV source region, covering the same field as in Fig. 2. The pointlike sources have been removed prior to the smoothing; they are overlaid as the faint green contours. Some spurious maxima in the diffuse emission are artifacts of the smoothing algorithm. The spurious maxima are those that appear pointlike but have no true pointlike (green contours) counterparts, e.g., the two pointlike maxima in the southeast. North is up, and east is to the left.

Thus, the 3EG contour fit ($E > 100$ MeV) is actually narrower ($E > 100$ MeV: $a = 18'.7$, $b = 15'.0$, $\phi = 67°$) than the one at $E > 1$ GeV. This is quite unusual and points toward an unfavorable (i.e., very soft) spectral index at energies above 1 GeV. In fact, the spectrum of 3EG J2033+4118 has already been studied for representation beyond the single–power-law fit (index of 1.96 ± 0.1 given in the 3EG catalog) and is significantly better represented if higher order spectral fits are performed. Bertsch et al. (2000) and Reimer & Bertsch (2001) concluded that in the case of 3EG J2033+4118 a double–power-law fit or a power-law fit with an exponential cutoff are more appropriate. This could partially explain the discrepancy between the EGRET flux and the HEGRA flux in a spectral energy distribution (see Fig. 3 in Aharonian et al. 2002), *if the MeV/GeV emission and the newly discovered TeV source are indeed directly related to the same astronomical object in the Cygnus region*. However, such a scenario is highly problematic in that after the index softens in the GeV range, it would then have to reharden to approximately -1.9 at the TeV energies observed by HEGRA. In our opinion, such an interpretation appears to be overly contrived.

Thus, while 3EG J2033+4118 and GeV J2035+4214/GRO J2034+4203 may be due to the same object(s), it is unlikely that the TeV source is *directly* related to any of them. 3EG J2033+4118 is probably connected with some subset of the ~2600 OB stars in the core of Cyg OB2, whereas TeV J2032+4131 could be related to the region coincident with an outlying OB subgroup, as shown in Figure 1. The sources can, however, still be considered indirectly related if the particles accelerated to GeV energies by the cumulative wind shocks from the Cyg OB2 core stars are reaccelerated to TeV energies by the collective wind shocks and turbulence in the region of the outlying OB subgroup. Verifying such a scenario will require deeper multiwavelength observations.

2.6. *OSSE*

During the *CGRO* mission (1991–1999), 11 separate hard X-ray/soft gamma-ray observations of the Cyg region with the OSSE detector included TeV J2032+4131. However, the field of view of OSSE was $3°.8 \times 11°.4$, and even using the Earth-occultation technique, one cannot resolve sources separated by less than $\sim 0°.5$, which happens to be the angular separation of the TeV source from Cyg X-3. The report of a 4.8 hr periodicity in the detected hard X-ray emission in this region by Matz et al. (1994) argues strongly for its association with Cyg X-3, and not with the TeV source. We also

TABLE 4
DETAILS OF THE MODEL PARAMETERS USED TO FIT THE BACKGROUND-SUBTRACTED DIFFUSE X-RAY SPECTRUM IN THE TeV SOURCE REGION

Parameter	Best Fit	1 σ Range	
		Range Below	Range Above
Optically Thin Plasma Model			
kT (keV)	11.3	-3.3	$+5.7$
Abundance	<1.2 (1 σ)	...	...
Normalization[a]	2.84×10^{-3}	-0.4×10^{-3}	$+0.4 \times 10^{-3}$
N(H) (cm^{-2})	1.5×10^{21}	-0.4×10^{21}	$+0.4 \times 10^{21}$
Power-Law Model			
Photon index	1.53	-0.11	$+0.12$
Normalization[b]	7.6×10^{-4}	-0.8×10^{-4}	$+1.0 \times 10^{-4}$
N(H) (cm^{-2})	1.8×10^{21}	-0.5×10^{21}	$+0.5 \times 10^{21}$

NOTES.—Because of poor statistics we cannot constrain the nature of the emission: thermal vs. power law. Both model fits yield approximately the same reduced $\chi^2 \sim 0.9$. Fluxes are as follows: 0.5–2.5 keV = 0.0006 photons cm^{-2} s^{-1}, 0.5–2.5 keV = 1.4×10^{-12} ergs cm^{-2} s^{-1}, 2.5–10 keV = 0.00045 photons cm^{-2} s^{-1}, and 2.5–10 keV = 3.6×10^{-12} ergs cm^{-2} s^{-1}.

[a] Units for normalization are $(10^{-14}/4\pi D^2) \int n_e n_{\rm H}\, dV$, where D is the distance.

[b] Units for normalization are photons keV^{-1} cm^{-2} s^{-1} at 1 keV.

reanalyzed the possible annihilation radiation from the TeV source region in OSSE data, but none was found: the 3 σ upper limits being 1.4×10^{-4} photons cm^{-2} s^{-1} for the 511 keV line and 5.0×10^{-4} photons cm^{-2} s^{-1} for the positronium continuum. (Care should be taken in comparing these limits with theoretical multiwavelength fits, since most models do not account for annihilation radiation.)

3. THE ATOMIC, MOLECULAR, AND DUST MORPHOLOGIES

The distribution of the local diffuse atomic, molecular, and dust material is important to understand, since it influences the damping and propagation of shocks produced by the stars in Cyg OB2 and can thus provide insight into the distribution and channeling of high-energy particles. It is also crucial to estimate the density of diffuse material in the region of the extended TeV source in order to be able to model the multiwavelength emissions. It should be stressed that distances inferred from gas velocities are very uncertain in the direction of Cyg OB2. Since our line of sight is nearly tangent to the solar circle, radial velocity increases only gradually with distance to a peak of $\sim$4 km s^{-1} at the subcentral distance of 1.4 kpc, then falls back to 0 km s^{-1} at 2.8 kpc, where our line of sight intersects the solar circle. The shallow velocity gradient causes severe blending of emission

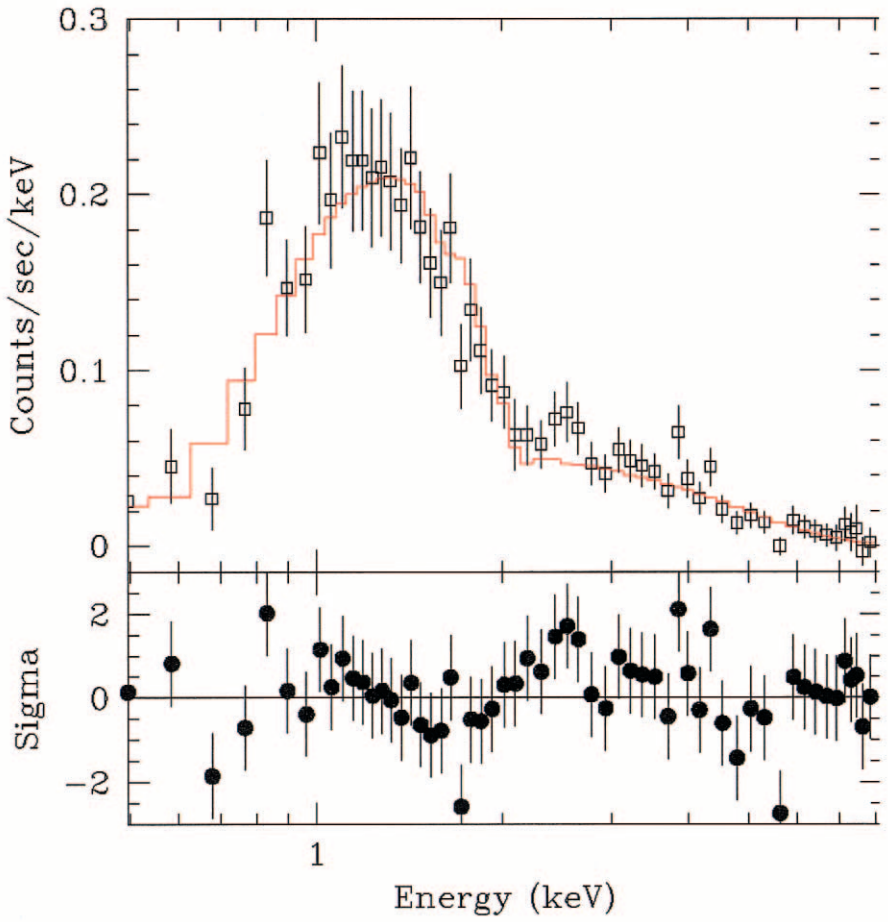

FIG. 4.—ACIS pulse-height spectrum of the diffuse emission in the TeV source region and best-fit optically thin plasma model, together with residuals in terms of σ. While there appear to be some systematic residuals, between 1 and 2 keV, for example, the data are in general well represented by the model, yielding a reduced χ^2 of 0.9. However, because of the poor statistics we cannot discriminate between a thermal vs. nonthermal model in the short 5 ks integration. *The power-law fit also yielded a reduced χ^2 of 0.9. Since the fit is qualitatively identical, it is not shown here.*

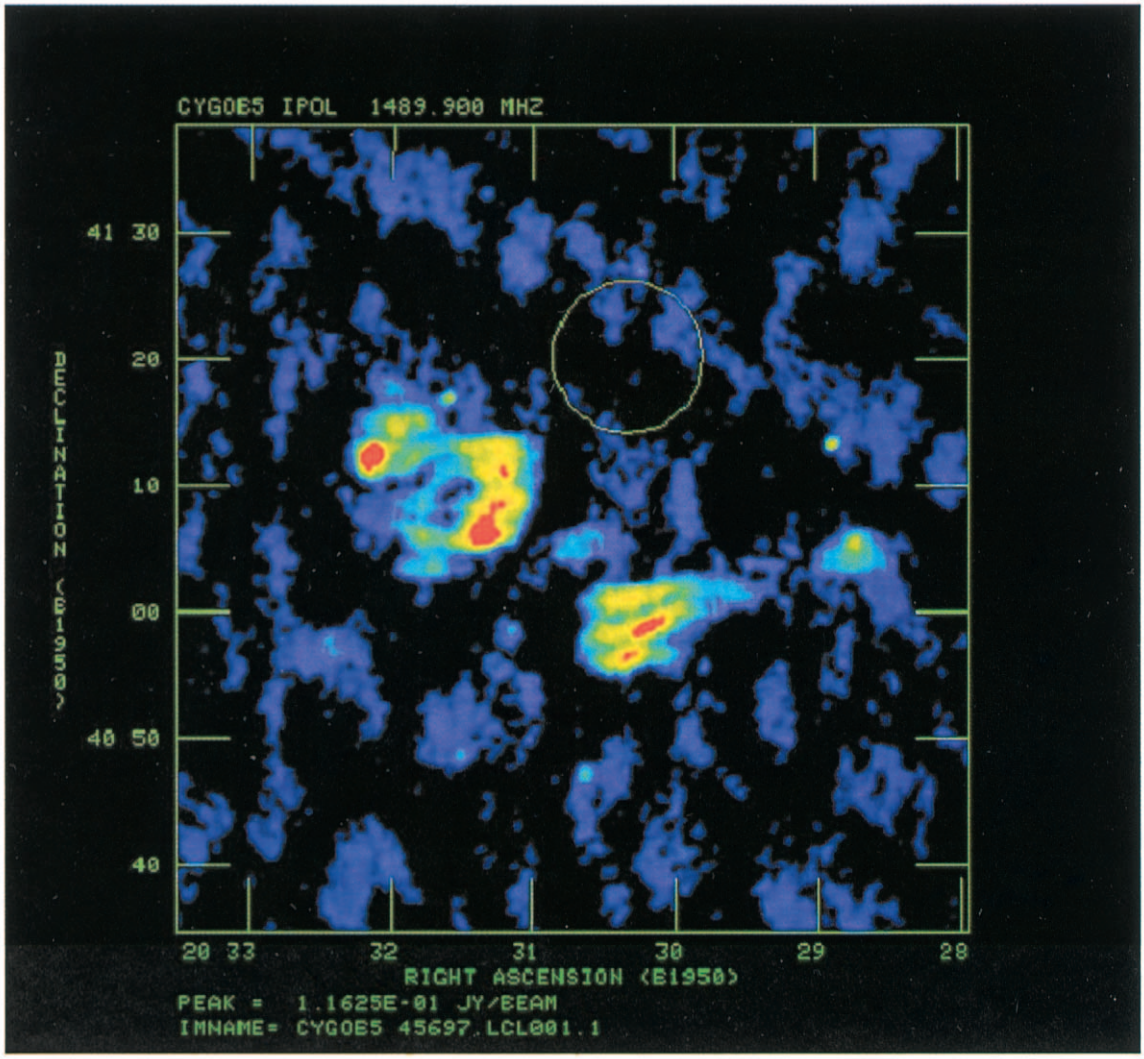

FIG. 5.—VLA D configuration radio image of the Cyg OB2 region. The green circle shows the 5′.6 radius extent of the diffuse TeV source TeV J2032+4131 reported by HEGRA (Rowell et al. 2002; Aharonian et al. 2002). The upper limit to the radio emission there at 1.49 GHz is <200 mJy.

from the local spiral arm, thought to be viewed tangentially in this direction. Figure 10 of Molnar et al. (1995) provides a very good overview of the Cyg OB2 line of sight.

3.1. *The* CO, H I, *and Ionized Hydrogen Distribution*

The CO $J = 1 \rightarrow 0$ rotational transition is the best general purpose tracer of molecular hydrogen gas. Using the Galactic CO survey of Dame, Hartmann, & Thaddeus (2001), we find good evidence for a molecular gas cavity centered roughly at $(l, b, v_{\rm lsr}) \sim (80.^\circ5, +1.^\circ8, +3$ km s$^{-1})$, $\sim 0.^\circ8$ northwest of the TeV source. The three orthogonal slices through the CO l-b-$v_{\rm lsr}$ data cube shown in Figure 6 suggest that the cavity is the center of an expanding shell with approximate dimensions marked by the dotted ellipses. The b-$v_{\rm lsr}$ (Fig. 6*a*) and l-$v_{\rm lsr}$ (Fig. 6*c*) maps further suggest that a front section of the shell may have been blown out toward us, with the remnants of that section seen at $v_{\rm lsr} \sim -30$ km s^{-1}. There are also hints in the l-b map (Fig. 6*b*) of other larger, partial shells roughly centered on Cyg OB2 (mainly in the denser gas at lower latitudes). Using a CO-to-H_2 mass conversion factor of 1.8×10^{20} cm^{-2} K^{-1} km^{-1} s (Dame et al. 2001) and adopting the distance of Cyg OB2 (1.7 kpc), the total H_2 mass in the vicinity of the shell ($l = 79^\circ$ to 81°, $b = 0.^\circ5$ to 3°, $v_{\rm lsr} = -12$ to $+6$ km s^{-1}) is $\sim 3.3 \times 10^5\ M_\odot$. This value should be considered an upper limit, since some emission from unrelated gas in the Local arm is probably blended in velocity with that from the shell.

We extracted the atomic hydrogen distribution from the Leiden-Dwingeloo H I survey (Burton & Hartmann 1994) and found a very interesting morphology with respect to the molecular hydrogen traced by the CO data: it appears that the molecular shell encloses a volume of atomic hydrogen, as shown in Figure 7. Note that in this figure the color is the intensity of 21 cm emission integrated from -6 to 10 km s^{-1}, and the contours are CO integrated over the same range. The l-$v_{\rm lsr}$ and b-$v_{\rm lsr}$ maps (Fig. 8) demonstrate that the region of enhanced H I fills the CO shell in l-b-$v_{\rm lsr}$ space. The enhanced H I may be disassociated H_2 from the molecular cloud that is currently being overtaken and destroyed by the expanding shell, powered possibly by an SNR or cumulative stellar

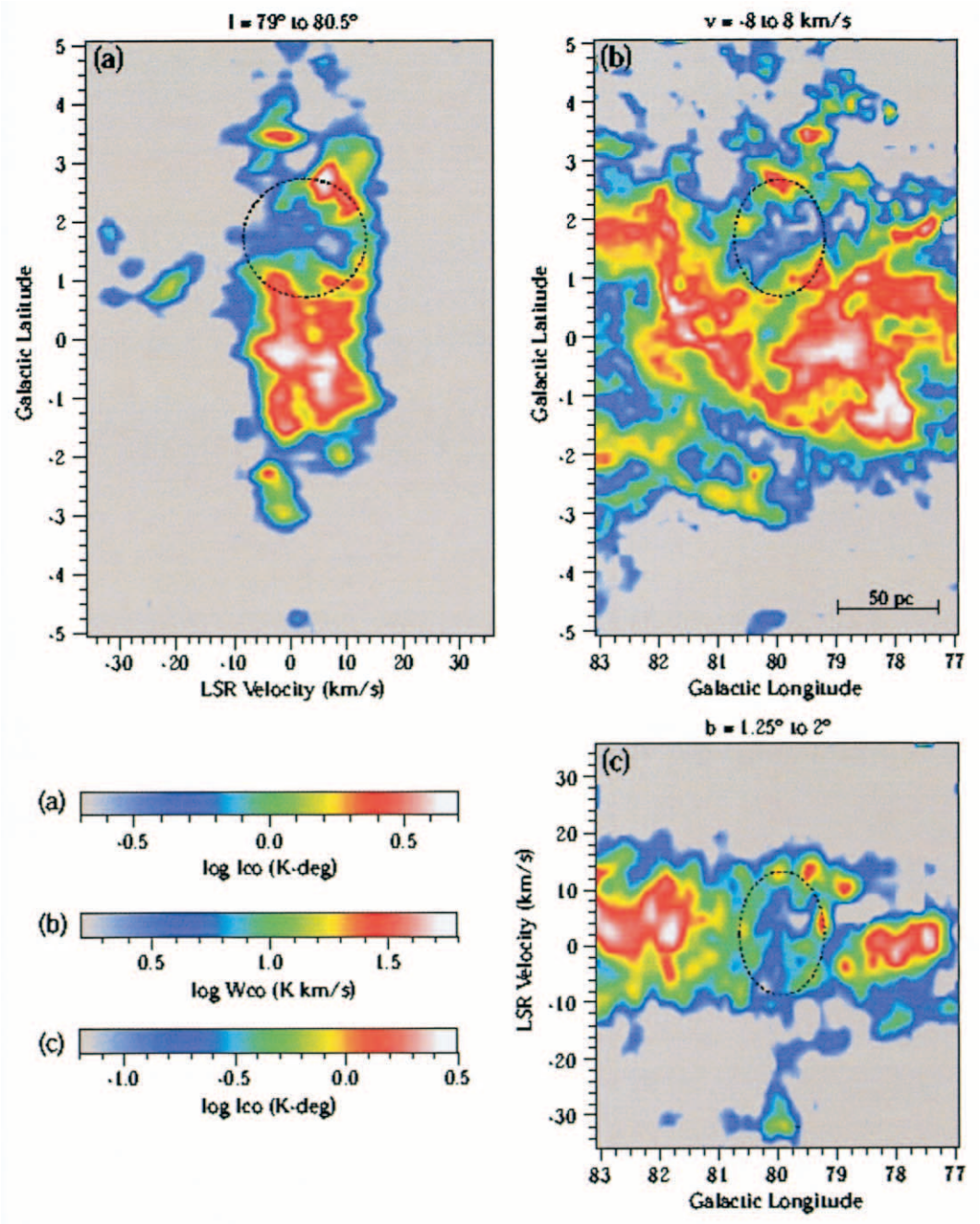

FIG. 6.—CO $J = 1 \rightarrow 0$ emission maps showing three orthogonal cuts through the l-b-$v_{\rm lsr}$ data cube. There is good evidence for an expanding cavity centered at approximately $(l,\ b) \sim (80.5,\ +1.8)$ in the velocity interval $v_{\rm lsr} \sim -8$ to $+13$ km s^{-1}. The dotted ellipse is simply a by-eye fit to the three dimensions of the shell. The l-b map also shows evidence for other partial shells roughly centered on Cyg OB2 (mainly toward lower latitude). In addition, the b-$v_{\rm lsr}$ and l-$v_{\rm lsr}$ maps suggest that a front section of the shell may have been blown out toward us, the remnants of that section perhaps seen at $v_{\rm lsr} \sim -30$ km s^{-1}.

cluster wind. Interestingly, Langston et al. (2000) have found a number of H II regions distributed on the periphery of this shell-like structure, indicating perhaps that material swept up by the expansion has triggered star formation there. Figure 9 displays the CO distribution overlaid on a large-scale 1.42 GHz radio emission map from the Canadian Galactic Plane Survey.

As a rough estimate of the gas density in the region of the TeV source, we calculate here the mean H_2 and H I densities within the shell along the line of sight to the source. Integrating the CO and 21 cm spectra toward the source over the range of -4 to $+10$ km s^{-1}, the estimated velocities of the front and back sides of the CO shell, yields

$$N(\mathrm{H_2}) = 4.2 \times 10^{20}\ \mathrm{H_2\ cm^{-2}} = 8.4 \times 10^{20}\ \mathrm{nucleons\ cm^{-2}}\ ,$$

$$N(\mathrm{H\ I}) = 32.2 \times 10^{20}\ \mathrm{H\ I\ cm^{-2}}\ .$$

The shell diameter is estimated to be 52 pc, but the path length through the shell along the line of sight to the TeV source is smaller, about 33 pc. Dividing the column densities

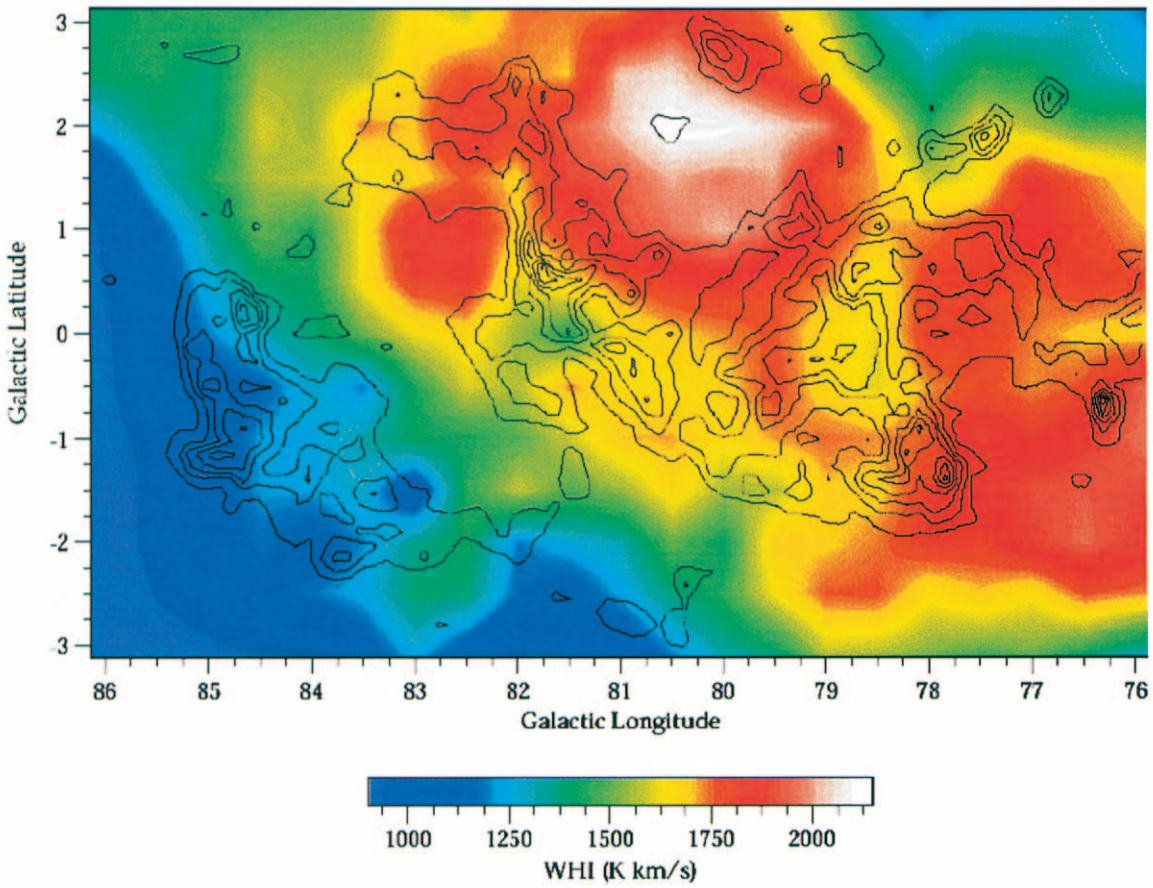

FIG. 7.—Similar to Fig. 6, but here the color scale is H I intensity (21 cm emission integrated from −6 to 10 km s^{-1}), and the contours are CO integrated over the same range, tracing the H_2 column density. Since the CO partial shell (centered at $[l, b] \sim [80.5, +1.8]$) encloses the H I (in *l*-*v* and *b*-*v* space also; see Fig. 8), a reasonable interpretation is that the ambient molecular hydrogen is being disassociated by the expanding shell. Note that Langston et al. (2000) have found a number of H II regions located at the periphery of the shell-like structure (see text).

by this length results in

$$n(\mathrm{H_2}) = 4.1\ \mathrm{H_2\ cm^{-2}} = 8.2\ \mathrm{nucleons\ cm^{-3}}\ ,$$

$$n(\mathrm{H\ I}) = 31.6\ \mathrm{H\ I\ cm^{-3}}\ .$$

Implicit in this calculation is the assumption that the CO emission over the velocity range of −4 to +10 km s^{-1} arises from a real localized object with velocities primarily due to expansion, not Galactic rotation. Otherwise, the velocity range of −4 to 10 km s^{-1} would correspond to ∼3.7 kpc along the line of sight. Molecular gas is so strongly clumped into large clouds that this assumption is reasonable; indeed, individual giant molecular clouds can have internal velocity widths comparable to the full velocity extent of the expanding shell proposed here. On the other hand, the H I gas is much more extended, and some of the 21 cm emission in the velocity range of the shell must be unrelated gas along the line of sight. The H I enhancement that apparently fills the molecular shell does appear superposed on a very substantial background; see, e.g., the color bar in Figure 7. We estimate that ∼65% of the 21 cm emission is actually unrelated to the shell. This reduces the n(H I) value estimated above to 11 cm^{-3} and the mean H_2 + H I density within the shell to ∼19 nucleons cm^{-3}.

To this value of density we must also add the density of ionized hydrogen in the region of the TeV source to arrive at an estimate of the total nucleon density. Unfortunately, a precise value for the ionized hydrogen content of the TeV source region alone is not available, but Huchtmeier & Wendker (1977) estimate that there is ∼2300 $M_\odot$ of ionized hydrogen within the extent of the entire Cyg OB2 association, or ∼10 protons cm^{-3} on average. The mean density of nucleons near the TeV source can then be approximated as $n_{\mathrm{tot}}(\mathrm{H_2} + \mathrm{H\ I} + \mathrm{proton}) \sim 30$ nucleons cm^{-3}.

3.2. 60 *and* 100 μm *IRAS Emission*

An examination of the reduced 60 and 100 μm *IRAS* data (e.g., Fig. 4*b* in Odenwald & Schwartz 1993; Fig. 1 in Le Duigou & Knödlseder 2002) clearly shows a dust void at the location of the TeV source. Odenwald & Schwartz (1993) argue that this void is due to the violent stellar environment of Cyg OB2: either the dust has been evacuated from Cyg OB2, and the TeV source region especially, or else it has been destroyed.

In summary, the molecular and dust maps show a low-density region at the location of the TeV source, most plausibly due to the action of the massive core stars of Cyg OB2, as well as the outlying OB subgroup coincident with the TeV source (Fig. 1). The co-added atomic+molecular+ionized density of the region of the TeV source is ∼30 nucleons cm^{-3}.

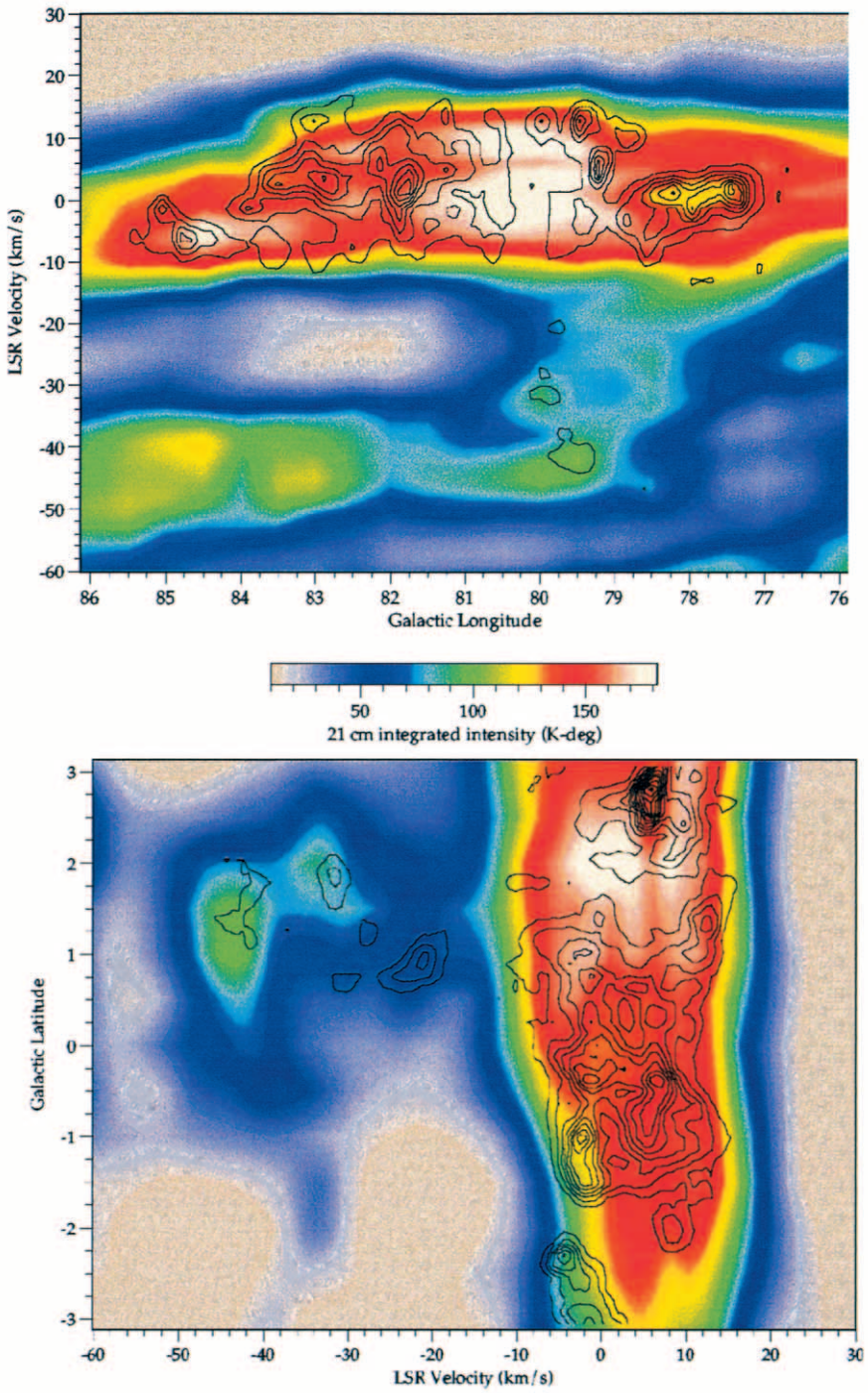

FIG. 8.—Similar to Fig. 7, but here the two panels show the two other orthogonal cuts through the H I (*color*) and CO (*contours*) data cubes. *Top*: Map of *l*-*v* integrated over the range $b = 1°$–$2°$; CO contour spacing is 0.5 K, starting at 0.5 K. *Bottom*: Map of *b*-*v* integrated over the range $l = 79.°5$–$80.°5$; CO contour spacing is 0.4 K, starting at 0.4 K. Note how the CO shell seen near $l \sim 80°$ in the top panel and near $b \sim 1.°8$ in the bottom panel coincides in velocity with an H I enhancement.

4. MODELING THE MULTIFREQUENCY EMISSION

Determining whether the TeV photons are dominantly produced by electronic or nuclear interactions is, of course, of fundamental importance in assessing whether Cyg OB2 can be considered a nucleonic GCR accelerator. In order to do this, we considered two main cases: one in which the TeV source is due predominantly to $\pi^0 \rightarrow \gamma\gamma$ emission from interactions of energetic nucleons and the other in which IC upscattering of cosmic microwave background (CMB) photons by relativistic electrons generates the bulk of observed gamma rays. (Considering the measured density of the TeV source region, the IC process will outshine electronic bremsstrahlung in the TeV gamma-ray domain, so we are justified in considering just the two cases mentioned.) A third case showing the effects of a lower density electron IC source was also calculated for the purpose of illustration.

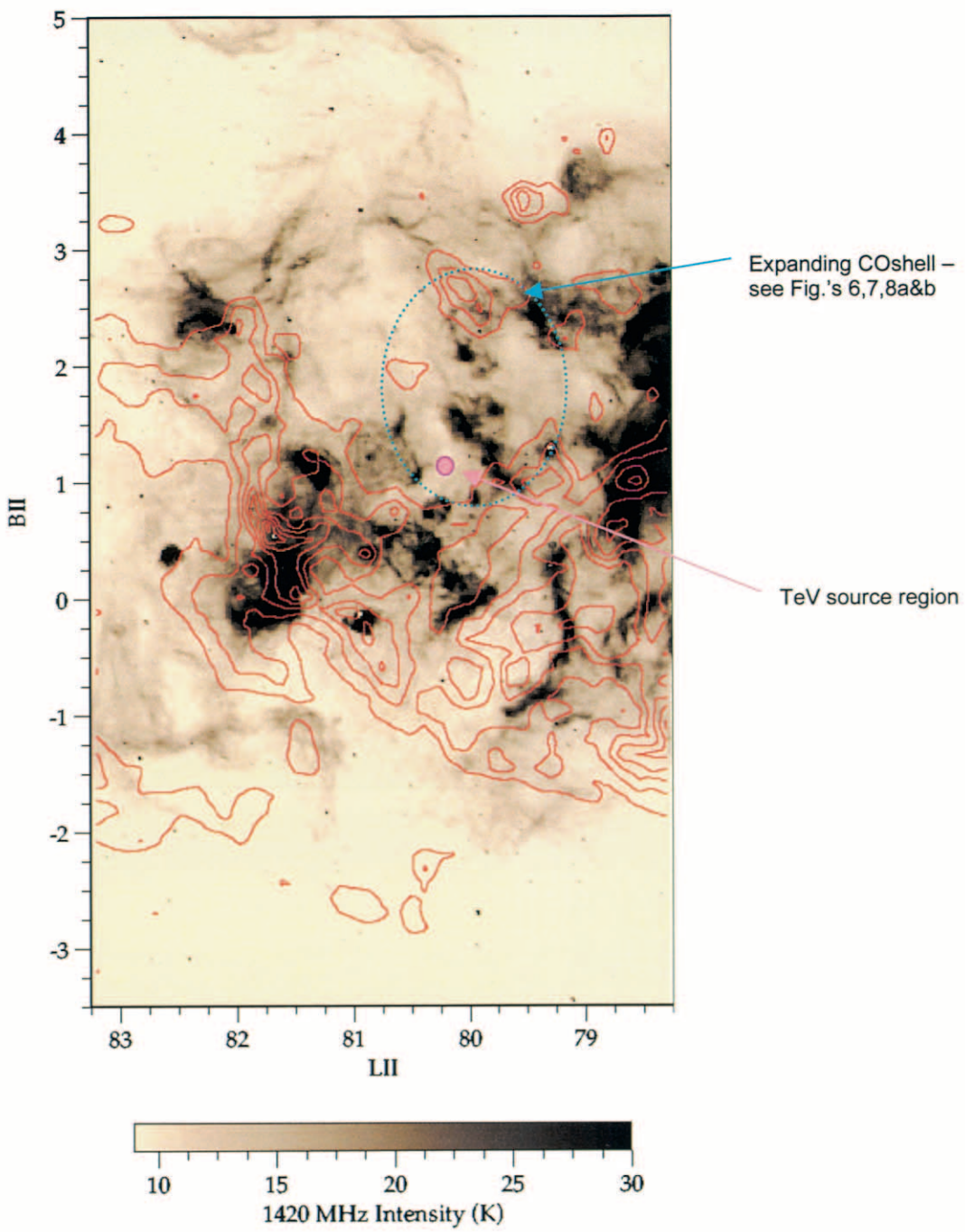

FIG. 9.—CO contours (-6 to 10 km s^{-1}) are shown overlaid on a 1.420 GHz intensity map obtained from the Canadian Galactic Plane Survey. The locations of the expanding shell (see Figs. 6–8) and the TeV source are marked. Note the possible relationship between the CO distribution and the radio structures in the region near $(l, b) \sim (80.5, +1.8)$.

We stress that we do not offer here any specific mechanism of accelerating the particles to such high energies, since this has been addressed already by several authors, e.g., Cesarsky & Montmerle (1983), Bykov & Fleishman (1992), Toptygin (1999), Bykov & Toptygin (2001), and Bykov (2001). We simply assess whether the multiband emissions of the TeV source region are more consistent with a predominantly hadronic versus a predominantly electronic origin, regardless of how the particles may be accelerated to such energies.

To do so, we assume that the putative acceleration mechanism (either shock and/or turbulent acceleration) generates a power-law spectrum of primary particles with a normalization, slope, and maximum energy chosen to agree with those determined empirically from the observed TeV spectrum. Following Aharonian et al. (2002), we take the spectral index as -1.9 and the maximum particle energy as 1 PeV. The required kinetic energy of the injected particles corresponds to only a fraction of a percent of the estimated kinetic energy available in the collective winds of Cyg OB2 (Lozinskaya et al. 2002).

The accelerated particles are assumed to be produced at a constant rate during the lifetime of the source, $\tau_{\rm source}$, which

is taken to be ~2.5 Myr (Knödlseder et al. 2000). The model results depend on the combination of $\tau_{\rm source}$ and environmental parameters (e.g., density, magnetic field) that determine the particle losses. However, the impact of the precise value of $\tau_{\rm source}$ is minor: as long as the particles have reached steady state ($\tau_{\rm cool} < \tau_{\rm source}$; as in the leptonic case below), the required energy in the injected particles is proportional to $\tau_{\rm source}$. When $\tau_{\rm cool} \gtrsim \tau_{\rm source}$, as in the hadronic case described below, a reduction in $\tau_{\rm source}$ would require a corresponding increase in the injection power to reproduce the observed radiation. Unlike the leptonic case, the required total energy of the injected particles is left unchanged.

The evolution of the injected particles is followed by integrating a transfer equation (e.g., Ginzburg & Syrovatskii 1969), as detailed in Miniati (2001, 2002). For the hadronic component, we include losses due to Coulomb collisions, bremsstrahlung, and *p-p* interactions, appropriate for the chosen maximum momentum, and for the leptonic part (*including the secondary* $e^{\pm}$'s), we consider Coulomb collisions, bremsstrahlung, synchrotron, and IC. The thermal gas, cosmic rays (CRs), and magnetic fields are taken as homogenous and equal to their average values. The radiation field for IC is dominated by the energy density in the CMB, and we neglect local contributions of both thermal and nonthermal (e.g., synchrotron) origin. In all cases, we assume a spherical source of radius = 5′.6 (or $r \sim 2.77$ pc at ~1.7 kpc) and mass = 66 $M_{\odot}$, corresponding to the above derived nucleon density of $n_{\rm tot} \sim 30$ cm^{-3} (except in the third case, in which we consider $n_{\rm tot} \sim 1$ cm^{-3} for illustrative purposes). In lieu of an empirically determined value of the magnetic field in Cyg OB2, we assume a field strength of 5 μG, a nominal Galactic value. *However, we stress that typical magnetic fields in young star-forming regions could be significantly higher* (e.g., Crutcher & Lai 2002).

The source term for the secondary electrons and positrons is derived self-consistently based on the evolved CR proton distribution function using the cross sections' model summarized in Moskalenko & Strong (1998). The calculation thus accurately tracks the radio through gamma-ray emission from secondary electrons resulting from the decays of charged muons and kaons produced in hadronic interactions. In particular, the code accounts for the two main secondary production channels: $p + p \rightarrow \pi^{\pm} + X$ and $p + p \rightarrow K^{\pm} + X$. Their relative contributions to production of the secondary electrons is a function of energy, so that the fraction of muons from K decay is ~8% at 100 GeV and ~19% at 1 TeV, and asymptotically approaches 27% at higher energies. Thus, the kaon channel cannot be neglected at the super-TeV energies considered here. The pions and kaons both decay eventually to electrons and positrons in the normal fashion (we do not show neutrinos for simplicity): $\pi^{\pm} \rightarrow \mu^{\pm} \rightarrow e^{\pm}$; $K^{\pm} \rightarrow \mu^{\pm} \rightarrow e^{\pm}$ (63.5%); or $K^{\pm} \rightarrow \pi^0 + \pi^{\pm} \rightarrow \gamma\gamma + \mu^{\pm} \rightarrow e^{\pm}$ (21.2%).

Importantly, we find that the broadband (especially radio) emission from the secondary electrons cannot be ignored, as has often been implicitly assumed in multiwavelength analyses of hadronic gamma-ray production in SNRs and other proposed GCR sources. This is because the age of the source (2–4 $\times 10^6$ yr) is much longer than the typical age of SNRs in their GCR acceleration phase (~10^4 yr), and thus, significantly more secondaries can accumulate in the source region (since their cooling time is longer than the few megayear age of the source).

The spectra resulting from our calculations are presented below in Figures 10–12 for three different cases with parameters as summarized below:

1. *With predominantly hadronic generation of TeV gamma rays*.—Shown in Figure 10, with $B = 5$ μG, $E_{p,\rm max} = 1$ PeV, $E_{e,\rm max} = 1$ PeV, $R_{e/p} = 0.01$, efficiency $\eta \sim E_{\rm CR}/E_{\rm kin} \sim 0.08\%$, and density = 30 cm^{-3}.
2. *With e^- IC generation of TeV gamma rays*.—Shown in Figure 11, with $B = 5$ μG, $E_{p,\rm max} = 1$ PeV; $E_{e,\rm max} = 1$ PeV, no protons, efficiency $\eta \sim E_{\rm CR}/E_{\rm kin} \sim 0.2\%$, and density = 30 cm^{-3}.
3. *With e^- IC generation of TeV gamma rays; low-density case*.—Shown in Figure 12, with $B = 5$ μG, $E_{p,\rm max} = 1$ PeV, $E_{e,\rm max} = 1$ PeV, no protons, efficiency $\eta \sim E_{\rm CR}/E_{\rm kin} \sim 0.2\%$, and density = 1 cm^{-3}.

In Figure 10 we report the scenario in which the TeV gamma rays have a hadronic origin. The plot shows the multiband spectra from radio to gamma-ray energies due to synchrotron, bremsstrahlung, and IC emission from primary electrons and secondary $e^{\pm}$, and neutral pion decay generated from *p-p* inelastic collisions. In this case, the emission from primary electrons is shown for comparison, and we assume a ratio of electrons to protons at relativistic energies of 0.01. While the TeV spectrum is well reproduced by the hadronic emission, the synchrotron emission due to secondaries generated in the same hadronic processes is below observational upper limits at both radio (1.4 GHz) and X-ray (keV range) frequencies. The predicted radio flux, in particular, is only a factor of 2–3 below the observed upper limit. With an assumed 5 μG magnetic field, the particles responsible for the radio synchrotron emission at 1.4 GHz have a Lorentz factor of the order of 10^4. Given the scaling of the synchrotron emission with magnetic field as $B^{1+\alpha}$, where $\alpha = 0.5$ is the spectral index, the magnetic field strength is allowed to be another factor of 2 or so higher before the radio upper limit is violated. This is, however, the most stringent case, as we discuss below. At these energies the timescale for bremsstrahlung losses is slightly shorter than the age of the source, meaning that this portion of the spectrum has basically reached steady state configuration (thick-target situation). A lower density would imply a lower rate of production of secondary particles through *p-p* collision and, therefore, of radio emission, despite the larger fraction of energy that would be radiated as synchrotron instead of bremsstrahlung radiation. In this case, for example, reduction in the density by an order of magnitude would allow a magnetic field as high as 20–30 μG. Finally, a higher gas density would enhance losses through bremsstrahlung, which would show up as a bump in the GeV gamma-ray range of the spectrum. Since this would occur at the expense of synchrotron emission, a higher magnetic field strength would again be allowed. This can be inferred by considering an approximate scaling for the radio flux as $B^{1.5}/n_{\rm tot}$.

The particle distribution of $e^{\pm}$ is characterized by two breaks at momenta of about 1 GeV/c and 1 TeV/c, marking, respectively, the transitions from losses dominated by Coulomb interaction to bremsstrahlung and from bremsstrahlung to the synchrotron/IC mechanism. These breaks, in particular the low-energy one, are actually extended, and therefore the spectral transitions are smooth. In addition, the spectra of secondaries start to cut off at momenta of a few TeV/c because of the cutoff in the parent proton spectrum and the average energy of a secondary in *p-p* inelastic

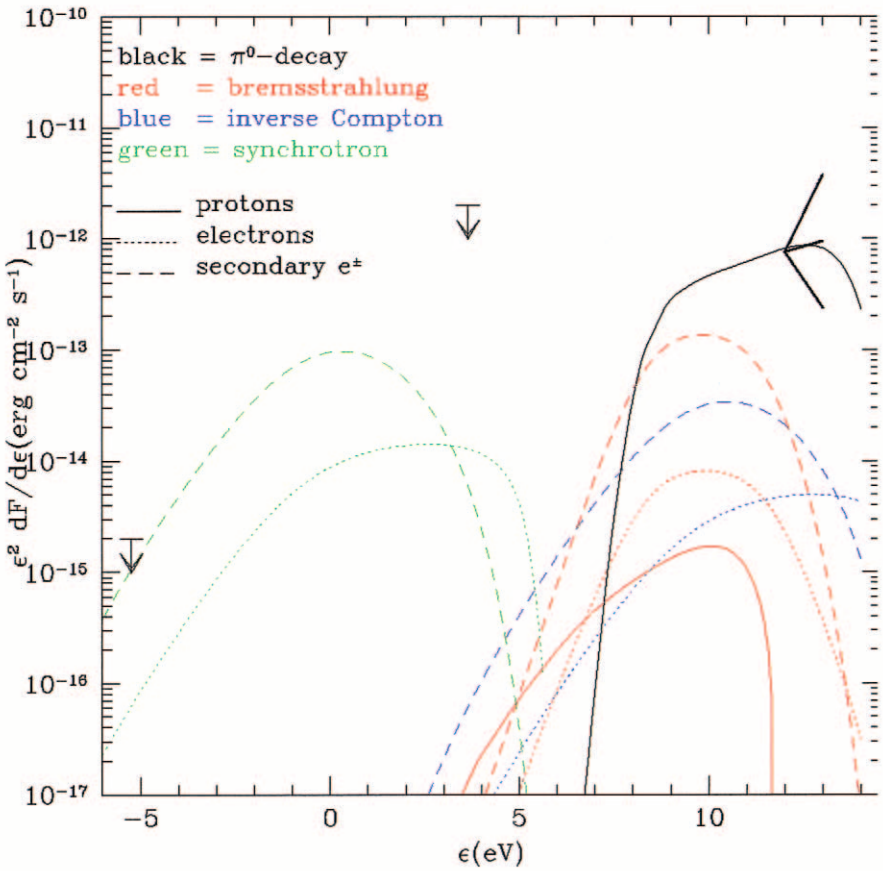

FIG. 10.—Simulated multiwavelength spectrum for the case in which the source TeV J2032+4131 has a predominantly hadronic origin. The ratio of primary electrons to protons was taken as 1%. A weak magnetic field of 5 μG was assumed, in line with the nominal Galactic value. Interestingly, the radio emission of the secondary electrons dominates the contribution from the primaries; this is because the age of the source (~2.5 Myr) exceeds the cooling time of the secondary $e^{\pm}$, and thus they simply accumulate in the source region. The injection efficiency (ratio of GCR energy to time-integrated wind power) is 0.08%. *Note that the measured X-ray flux is taken here as an upper limit to the nonthermal component alone. Deeper X-ray and radio observations will help resolve the diffuse nonthermal components, which could then be directly compared with the simulated spectrum shown here.*

collisions (e.g., Mannheim & Schlickeiser 1994). Note that given the finite lifetime of the source, a steady state configuration has not been reached for all particle energies. In addition, a fraction of the energy is dissipated through Coulomb collision by particles with momenta below approximately a few GeV/c. This implies that the total luminosity of the secondaries is less than half of that produced by the decay of neutral pions.

In Figure 11 we consider the case in which the TeV flux arises from electron IC emission. Thus, as compared to the previous case, we increased the injected population of electrons by a factor of more than 200 (hadronic contributions are not shown here for clarity). Since the background gas density and magnetic fields are unchanged with respect to the previous case, the same description of the spectral features applies here as well. It is obvious from the figure that in this case both radio and X-ray upper limits are violated. Particularly, in order to reconcile the predicted and measured radio flux at 1.4 GHz would require a magnetic field at the level of ~1 μG, which is below the Galactic average.

Finally, Figure 12 shows the same case as in Figure 11 but now—for illustration only—using a lower gas density of 1 cm^{-3}. Now, the radio-emitting particles are not affected by bremsstrahlung losses (thin target), which is reflected in the sharper breaks in the radiation spectra. Because of the limited lifetime of the source (2.4 Myr), the synchrotron emission is increased by only a factor of ~3, which implies only a slightly more stringent upper limit on the magnetic field strength with respect to the previous case.

Clearly, even with the low adopted magnetic field of 5 μG, electrons are disfavored as the dominant source of the TeV gamma rays, since both the radio and X-ray upper limits are violated by the synchrotron emission (Figs. 11 and 12).

It is often stated that a massive and dense cloud is needed to explain the TeV emission as being hadronic in origin. However, there are two main ingredients that determine the hadronic luminosity of a given source: one is indeed the value of the ambient density, but the other is the source's local CR power. We find that the low intensity of this TeV source is easily accommodated by the combination of the empirically determined density of just ~30 nucleons cm^{-3} at the source site and the ~0.1% CR acceleration efficiency (i.e., ~10^{36} ergs s^{-1} in CRs locally). There is no need to invoke a very massive and/or dense molecular cloud at the TeV source site in order to explain the multiwavelength emissions in terms of p-p interactions.

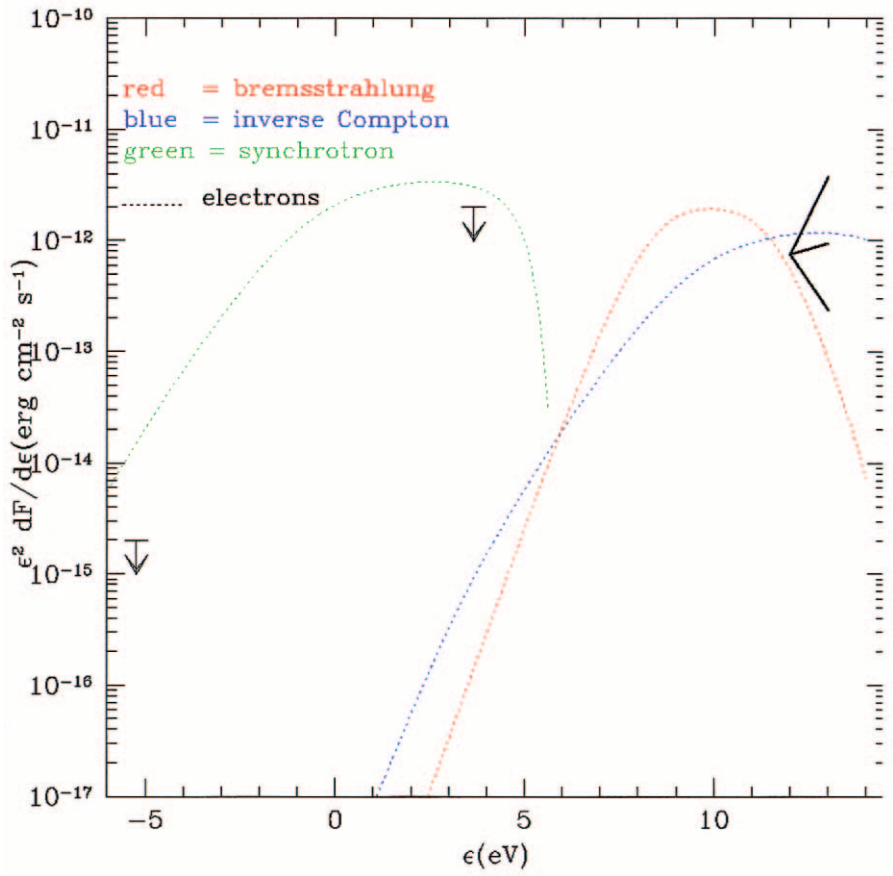

FIG. 11.—Simulated multiwavelength spectrum for the case in which the source TeV J2032+4131 has a purely electronic origin. A weak magnetic field of 5 μG was assumed, in line with the nominal Galactic value. The injection efficiency (ratio of required GCR energy to time-integrated wind power) in this case is 0.2%. *Note that both the X-ray and radio upper limits are violated, and thus an electronic origin for TeV J2032+4131 is disfavored.* If a lower magnetic field exists in the TeV source region, this would, of course, decrease the synchrotron emission (*green curve*) and could allow for an electronic model. However, Crutcher & Lai (2002) find that magnetic fields in young star-forming regions are typically even higher—and not lower—than the nominal Galactic value of 5 μG we have used here. *Note that, as in the previous figure, the measured X-ray flux is taken here as an upper limit to the nonthermal component alone. Deeper X-ray and radio observations will help resolve the diffuse nonthermal components, which could then be directly compared with the simulated spectrum shown here.*

5. SUMMARY AND CONCLUSIONS

We have carried out follow-up X-ray and radio observations of the extended and steady unidentified TeV source region recently reported by the HEGRA collaboration in Cyg OB2, the most massive OB association known in the Galaxy. The new data taken together with the reexamination of archival radio, X-ray, CO, H I, and *IRAS* data suggest that collective turbulence and large-scale shocks due to the interacting supersonic winds of the ~2600 core OB stars of Cyg OB2, with those of an outlying subgroup of powerful OB stars in Cyg OB2, are likely responsible for the observed very high energy gamma-ray emissions (Fig. 1). Since new analysis of 2002 HEGRA data confirms the extended and steady nature of the TeV source (Horns & Rowell 2003), a blazar-like hypothesis for the origin of the TeV flux, such as that explored by Mukerjee et al. (2003), is now untenable. It is, however, possible that the extended TeV source is actually composed of multiple, nearby steady pointlike TeV sources such as may result from a concentration of "target" stars immersed in an intense CR bath (e.g., Romero & Torres 2003). Higher spatial resolution TeV observations, such as those made possible by the High-Energy Stereoscopic System (HESS), may help in resolving this issue. The suggestion that the TeV source may possibly be associated with Cyg X-3 (e.g., Aharonian et al. 2002) is also difficult to reconcile with the fact that Cyg X-3's jets lie at $\lesssim 14^\circ$ to the line of sight: the deprojected distance between Cyg X-3 and the TeV source at Cyg X-3's location (~9 kpc distant) appears to be too large to support such a hypothesis.

We have carried out detailed simulations of the multifrequency spectra of the extended TeV source and favor a scenario in which the TeV gamma rays are dominantly of a nucleonic, rather than an electronic, origin. A magnetic field of just 5 μG at the TeV source site would rule against the possibility of an electronic origin for the TeV flux (Fig. 11). Since much higher fields are known to exist in young stellar associations (e.g., Crutcher & Lai 2002), a predominantly hadronic source is favored (Fig. 10). We find no need to invoke a dense and/or massive molecular cloud at the extended TeV source site to explain the multifrequency emissions in terms of accelerated hadrons.

Deeper radio and X-ray observations would be useful in order to separate the nonthermal versus thermal components of the diffuse emissions so that straightforward comparisons with multiwavelength simulations can be made. A determination of the Cyg OB2 magnetic field in this region would also place strong constraints on TeV source models and is highly desirable. Further high-sensitivity infrared observations, such as those already carried out by Comerón

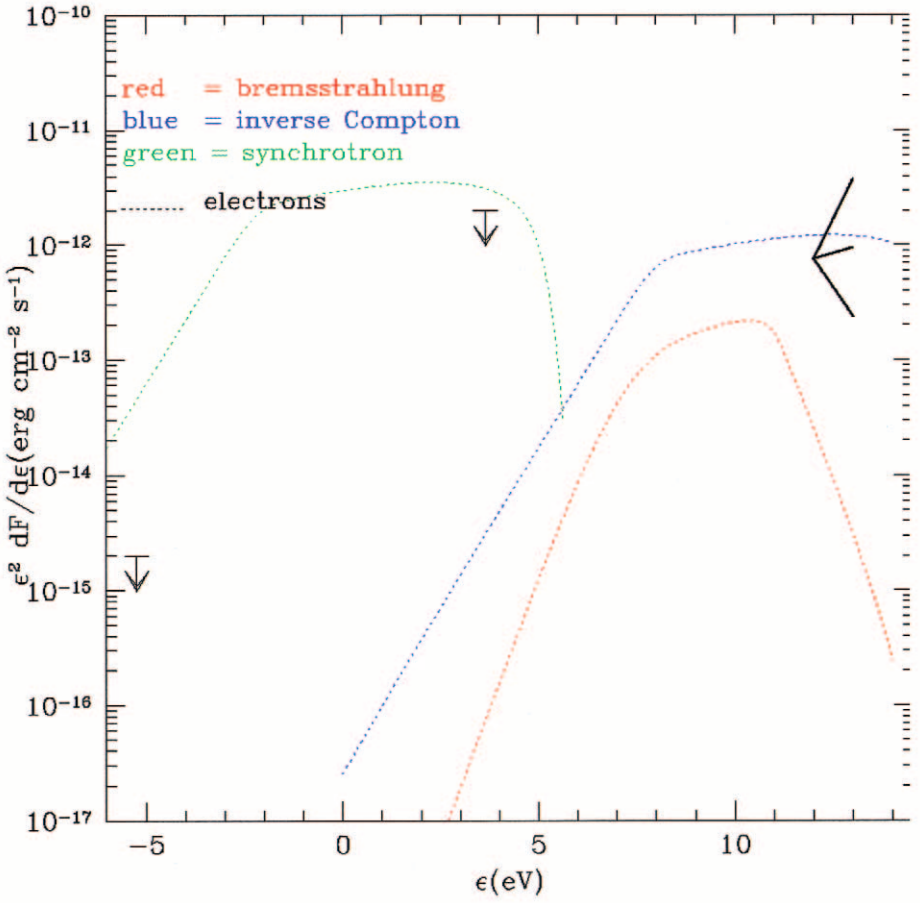

FIG. 12.—Same as Fig. 11, except a density of 1 cm^{-3} is used instead of the empirically determined ~30 cm^{-3}

et al. (2002), would be very useful in order to make an accurate census of the OB stars toward the highly extincted region of the extended TeV source. Of course, future observations by the *Gamma-Ray Large Area Space Telescope* and the next generation of stereoscopic Cerenkov telescopes (HESS, VERITAS, etc.) will be critical in exposing the nature of this mysterious very high energy gamma-ray source.

We are indebted to Harvey Tananbaum and the *Chandra* X-Ray Center in granting us DDT time and to the VLA for allowing the scheduling of the B configuration observation on such short notice. Discussions with, and information from, Peter Biermann, Dieter Horns, Jurgen Knödlseder, Henric Krawczynski, Maura McLaughlin, Thierry Montmerle, Etienne Parizot, Jerome Rodriguez, Gavin Rowell, Diego Torres, Bulent Uyaniker, Mike Shara, David Thompson, Heinz Wendker, Dave Zurek, and Fernando Comerón are appreciated. Y. M. B. acknowledges the support of the *Chandra* project, NASA contract NAS8-39073. Study of this extended and nonvariable TeV gamma-ray source is also supported by *Chandra* grant DD2-3020X. The use of the HEASARC archive at the Goddard Space Flight Center, the NASA Astrophysics Data System, and the Canadian Galactic Plane Survey was invaluable to this study.

REFERENCES

Aharonian, F., et al. 2002, A&A, 393, L37
Alibés, A., Labay, J., & Canal, R. 2002, ApJ, 571, 326
Anchordoqui, L. A., Romero, G. E., & Combi, J. A. 1999, Phys. Rev. D, 60, 103001
Anders, E., & Grevesse, N. 1989, Geochim. Cosmochim. Acta, 53, 197
Benaglia, P., Romero, G. E., Stevens, I. R., & Torres, D. F. 2001, A&A, 366, 605
Berezhko, E. G., Puehlhofer, G., & Völk, H. J. 2003, A&A, 400, 971
Bertsch, D. L., et al. 2000, in AIP Conf. Ser. 510, Proc. 5th Compton Symp., ed. M. L. McConnell & J. M. Ryan (Melville: AIP), 504
Bruhweiler, F. C., Gull, T. R., Kafatos, M., & Sofia, S. 1980, ApJ, 238, L27
Burton, W. B., & Hartmann, D. 1994, Ap&SS, 217, 189
Butt, Y. M., Torres, D. F., Romero, G. E., Dame, T. M., & Combi, J. A. 2002, Nature, 418, 499
Bykov, A. 2001, Space Sci. Rev., 99, 317
Bykov, A. M., & Fleishman, G. D. 1992, MNRAS, 255, 269
Bykov, A. M., & Toptygin, I. N. 2001, Astron. Lett., 27, 625
Cassé, M., & Paul, J. A. 1980, ApJ, 237, 236
Cesarsky, C. J., & Montmerle, T. 1983, Space Sci. Rev., 36, 173
Chen, W., White, R. L., & Bertsch, D. 1996, A&AS, 120, 423
Chu, Y.-H. 1997, AJ, 113, 1815
Comerón, F., et al. 2002, A&A, 389, 874
Contreras, M. E., Rodriguez, L. F., Tapia, M., Cardini, D., Emanuele, A., Badiali, M., & Persi, P. 1997, ApJ, 488, L153
Crutcher, R. M., & Lai, S.-P. 2002, in ASP Conf. Ser. 267, Hot Star Workshop III: The Earliest Stages of Massive Star Birth, ed. P. A. Crowther (San Francisco: ASP), 61
Dame, T. M., Hartmann, D., & Thaddeus, P. 2001, ApJ, 547, 792
Dar, A. & Plaga, R. 1999, A&A, 349, 259
Drury, L. O'C., et al. 2001, Space Sci. Rev., 99, 329
Ellison, D., Berezhko, E., & Baring, M. 2000, ApJ, 540, 292
Erlykin, A. D., & Wolfendale, A. W. 2003, J. Phys. G, 29, 709
Gaisser, T., Protheroe, R., & Stanev, T. 1998, ApJ, 492, 219
Ginzburg, V. L., & Syrovatskii, S. I. 1969, The Origin of Cosmic Rays (New York: Gordon & Breach)
Hartman, R. C., et al. 1999, ApJS, 123, 79

Heiles, C. 1979, ApJ, 229, 533
Horns, D., & Rowell, G. 2003, in Proc. 2d VERITAS Symp. on TeV Astrophysics of Extragalactic Sources, ed. M. Catanese & T. C. Weekes (New York: North-Holland), in press
Huchtmeier, W. K., & Wendker, H. J. 1977, A&A, 58, 197
Itoh, C., et al. 2002, A&A, 396, L1
———. 2003, ApJ, 584, L65
Kafatos, M., Bruhweiler, F. C., & Sofia, S. 1981, Proc. 17th Int. Cosmic-Ray Conf. (Paris), 2, 222
Knödlseder, J. 2000, A&A, 360, 539
———. 2003, in IAU Symp. 212, A Massive Star Odyssey from Main Sequence to Supernova, ed. K. A. van der Hucht, A. Herrero, & C. Esteban (San Francisco: ASP), 505
Lamb, R. C., & Macomb, D. J. 1997, ApJ, 488, 872
Langston, G., et al. 2000, AJ, 119, 2801
Le Duigou, J.-M., & Knödlseder, J. 2002, A&A, 392, 869
Lozinskaya, T. A., Pravdikova, V. V., & Finoguenov, A. V. 2002, Astron. Lett., 28, 223
Mac Low, M.-M., & McCray, M. 1988, ApJ, 324, 776
Mannheim, K., & Schlickeiser, R. 1994, A&A, 286, 983
Markevitch, M., et al. 2003, ApJ, 583, 70
Massey, P., & Thompson, A. B. 1991, AJ, 101, 1408
Mattox, J. R., Hartman, R. C., & Reimer, O. 2001, ApJS, 135, 155
Matz, S. M., Grabelsky, D. A., Purcell, W. R., Ulmer, M. P., Johnson, W. N., Kinzer, R. L., Kurfess, J. D., & Strickman, M. S. 1994, in AIP Conf. Proc. 308, Hard X-Ray Variability of Cygnus X-3, The Evolution of X-Ray Binaries, ed. S. Holt & C. S. Day (New York: AIP), 263
McCray, R., & Kafatos, M. 1987, ApJ, 317, 190
McLaughlin, M. A., Mattox, J. R., Cordes, J. M., & Thompson, D. J. 1996, ApJ, 473, 763
Miniati, F. 2001, Comput. Phys. Commun., 141, 17
———. 2002, MNRAS, 337, 199
Molnar, L. A., Mutel, R. L., Reid, M. J., & Johnston, K. J. 1995, ApJ, 438, 708
Montmerle, T. 1979, ApJ, 231, 95
Moskalenko, I. V., & Strong, A. W. 1998, ApJ, 493, 694
Mukerjee, R., Halpern, J. P., Gotthelf, E. V., Eracleous, M., & Mirabal, N. 2003, ApJ, 589, 487
Muraishi, H., et al. 2000, A&A, 354, L57
Odenwald, S. F., & Schwartz, P. R. 1993, ApJ, 405, 706
Parizot, E. 2003, in Proc. XXII Moriond Astrophys. Meeting, The Gamma-Ray Universe, ed. A. Goldwurm, D. Neumann, & J. Tran Thanh Van (Gif-sur-Yvette: Editions Frontières), in press
Prinja, R. K., Barlow, M. J., & Howarth, I. 1990, ApJ, 361, 607
Ramaty, R., Lingenfelter, R. E., & Kozlovsky, B. 2001, Space Sci. Rev., 99, 51
Reddish, V. C., Lawrence, L. C., & Pratt, N. M. 1966, Publ. R. Obs. Edinburgh, 5, 111
Reimer, O., & Bertsch, D. L. 2001, Proc. 27th Int. Cosmic-Ray Conf. (Hamburg), 6, 2546
Reimer, O., Dingus, B. L., & Nolan, P. L. 1997, Proc. 25th Int. Cosmic-Ray Conf. (Durban), 3, 97
Reimer, O., & Pohl, M. 2002, A&A, 390, L43
Romero, G. E., Benaglia, P., & Torres, D. F. 1999, A&A, 348, 868
Romero, G. E., & Torres, D. F. 2003, ApJ, 586, L33
Rowell, G., et al. 2003, in Proc. XXII Moriond Astrophys. Meeting, The Gamma-Ray Universe, ed. A. Goldwurm, D. Neumann, & J. Tran Thanh Van (Gif-sur-Yvette: Editions Frontières), in press
Tompkins, W. F. 1999, Ph.D. thesis, Stanford Univ.
Toptygin, I. N. 1999, Astron. Lett., 25, 814
Torres, D. F., Romero, G. E., Combi, J. A., Benaglia, P., Anderach, H., & Punsly, B. 2001, A&A, 370, 468
Torres, D. F., Romero, G. E., Dame, T. M., Combi, J. A., & Butt, Y. M. 2003, Phys. Rep., 382, 303
Uyaniker, B., Fürst, E., Reich, W., Aschenbach, B., & Wielebinski, R. 2001, A&A, 371, 675
Vacca, W. D., Garmany, C. D., & Schull, J. M. 1996, ApJ, 460, 914
Vink, J. S., de Koter, A., & Lamers, H. J. G. L. M. 2000, A&A, 362, 295
Waldron, W. L., Corcoran, M. F., Drake, S. A., & Smale, A. P. 1998, ApJS, 118, 217
White, R., & Chen W. 1992, ApJ, 387, L81

Note added in proof.—Shortly after this paper, a very relevant paper on Cygnus OB2 will be published (M. M. Hanson, ApJ, 597, in press [2003]).